Stony Brook University

Finding Fluorescent Needles in the Cardiac Haystack: Tracking the location and fate of hMSCs with quantum dots for electrical and mechanical repair of damaged myocardium

A Dissertation Presented

by

Amy Beth Rosen

to

The Graduate School

in Partial Fulfillment of the

Requirements

for the Degree of

Doctor of Philosophy

in

Biomedical Engineering

Stony Brook University

May 2007

Stony Brook University

The Graduate School

Amy Beth Rosen

We, the dissertation committee for the above candidate for the

Doctor of Philosophy degree,

hereby recommend acceptance of this dissertation.

Ira S. Cohen, M.D., Ph.D., Dissertation Advisor
Leading Professor, Department of Physiology and Biophysics
Stony Brook University

Emilia Entcheva, Ph.D., Chairperson of Defense
Assistant Professor, Department of Biomedical Engineering
Stony Brook University

Peter R. Brink, Ph.D.
Professor and Chairman, Department of Physiology and Biophysics
Stony Brook University

Glenn R. Gaudette, Ph.D.
Assistant Professor, Department of Biomedical Engineering
Worcester Polytechnic Institute

This dissertation is accepted by the Graduate School

Lawrence Martin
Dean of the Graduate School

Abstract of the Dissertation

Finding Fluorescent Needles in the Cardiac Haystack: Tracking the location and fate of hMSCs with quantum dots for electrical and mechanical repair of damaged myocardium

by

Amy Beth Rosen

Doctor of Philosophy

in

Biomedical Engineering

Stony Brook University

2007

Adult myocardium has long been considered an amitotic tissue, incapable of self-repair after injury. Stem cells now show promise for restoring mechanical and electrical function to damaged heart tissue. One major limitation to studying the mechanism of stem cell action *in vivo,* however, has been the difficulty of labeling and then tracking the cells delivered in animal models. Traditional fluorescent proteins and dyes fail to illuminate exogenous cells amidst the high levels of autofluorescence in the heart. Non-invasive cell tracking methods have been developed but suffer from poor resolution. In order to fully understand the spatiotemporal distribution of stem cell clusters in the heart, as well as determine the fate of these delivered cells, the ideal cell tracking method must overcome these challenges. We have developed a novel

technique using quantum dot (QD) fluorescent nanoparticles to track stem cells delivered *in vivo*. Our approach uniformly loads QDs into human mesenchymal stem cells (hMSCs) with no observed effect on cell proliferation or gene expression. Labeled cells maintain the ability to differentiate *in vitro* along adipogenic and osteogenic lineages, and terminally differentiated cells retain the QDs. QD-hMSCs can be delivered to myocardium *in vivo* and easily identified in histologic sections without immunostaining or effects from autofluorescence. After injecting QD-hMSCs into the rat ventricle *in vivo*, we have generated 3-D reconstructions of their complete distribution with single-cell resolution. Furthermore, we have tracked the fate of QD-hMSCs eight weeks after delivery to the canine heart on an extracellular matrix patch. QD-hMSCs were found to differentiate along an endothelial lineage, suggesting participation by these cells in vasculogenesis. We also identified expression of cardiac-specific markers in cells containing the QD label; in some cases, QD-hMSC-derived cells were found with morphologic hallmarks of mature cardiac myocytes, suggesting they can terminally differentiate into this cell type. In summary, this novel technique of stem cell labeling with QDs provides a robust method for tracking the location and fate of stem cells both *in vitro* and after delivery *in vivo*.

Table of Contents

List of Figures

List of Tables

Acknowledgements

Science is a living, growing field. I am foremost indebted to the thousands of scientists who have laid the groundwork for the research we engage in today. It has been an honor and privilege to be a part of science's rich tradition and contribute my (albeit small) piece to the puzzle.

None of the work contained within these pages would have been possible without the superb mentorship of Ira Cohen. Over the past three years, Ira has instructed me in the areas of cardiac electrophysiology, cardiac pathology, stem cell biology and the practice of science in general. Ira's love for problem solving and curious nature has pushed me to think creatively about problems and draw solutions from outside disciplines. He has been a constant source of support both scientifically and personally. His intelligence, generosity, flexibility, friendship and commitment to education make him the archetype thesis advisor. In his lab, I have had the opportunity to truly have fun doing research and I will always be grateful to him for this experience.

I also owe a tremendous amount to Glenn Gaudette. His unwaveringly strict scientific standards have inspired me to set a very high bar for myself. Glenn trained me in surgical techniques, experimental design, and cardiac biomechanics. Like Ira, Glenn is extremely creative and thoughtful about scientific problems, and has taught me to critically interpret published data and to scrutinize my own data as well.

Much of my research focused on histologic analysis and I often consulted Peter Brink for his mastery in this area. Peter's know-how proved essential to the execution of my project aims. Likewise, Emilia Entcheva was a great teacher of quantitative image analysis and microscopic techniques. In a course she taught in my first year of graduate school (Cell and Molecular Imaging), I learned the fundamentals of image processing that would later become the keystone of this dissertation.

Many other members of Ira's lab contributed to this work. Damon Kelly, a post-doctoral fellow, provided valuable assistance with Matlab programming and Adam Schuldt, a fellow MSTP graduate student, performed all of the rodent surgeries with extraordinary skill. Damon, Adam, and our other labmate Vic Tselentakis were daily sources of counsel and camaraderie and I had a lot of fun sharing an office with them. Jia Lu did the patch clamp studies and Irina Potapova performed the mitochondrial dehydrogenase assay. Joan Zuckerman, Diane Tripani and Mickey Parris offered precious technical assistance. David Rubinstein in Dr. Molly Frame's lab provided materials and assistance for creating the phantom mold discussed in Chapter 4.4.

I have also been fortunate to collaborate with talented scientists at Columbia University, including: Michael Rosen, Richard Robinson, Peter Danilo, Lev Protas, Alexei Plotnikov and Iryna Shlapakova, all from the Department of Pharmacology.

Working with Peter Davies and Brian Helmke as an undergraduate at the University of Pennsylvania was the defining experience in my decision to purse a Ph.D. I am forever beholden to both Peter and Brian for their mentorship, guidance and friendship. Diane Cabelli, a Chemist at Brookhaven National Laboratories opened her lab to me as a naïve high school student, encouraged me, and showed me that driven, talented women can balance a successful scientific career with a happy family life.

These three brilliant people are my role models for how to conduct oneself as a scientist.

Theresa Scrocco (one of my elementary school teachers) played a major role in my life's trajectory by providing my first exposure to research, and instilling in me a love for reading.

Many other people at Stony Brook have dedicated time, energy and resources to helping me complete this dissertation. I am grateful to the staff in the Physiology and BME Departments: Judy Samarel, Melanie Bonnette, Charlotte Duff, Robin Green, and Anne Marie Dusatko. Melanie in particular went above and beyond her call of duty on my behalf numerous times and I truly appreciate her work. Since beginning the Medical Scientist Training Program in 2002, Carron Kaufman and Michael Frohman have helped at every step along the way and I appreciate all of their efforts. I'd also like to acknowledge and thank Carrie-Ann Miller, Sharon Pavulaan, Ann Sutton, Sally Sternglanz, Doreen Aveni, Diane Aveni, the faculty, and the undergraduate and graduate students from the Women in Science and Engineering program for their friendship, support and inspiration.

The most important people to me, however, are those with whom I had the least interaction on a day-to-day basis in the lab. My family has been cheerleading behind me since my first day of elementary school. My parents raised me to value education and perpetually seek out new academic challenges. My mother, Barbara, inspired me to be compassionate and well-read and my father, Alvin, taught me to question everything. My sister, Stefanie, my hero in life, has taught me how to set goals and achieve them. I only hope I can match half of her diligence, commitment and drive. My grandmother, Sylvia and my brother-in-law, Benjamin (a constant source of laughs) have shown immeasurable love and support for me and I appreciate them immensely. Finally, from the bottom of my heart I thank Alex Kontorovich for his love, friendship, humor, brilliance, music, meals, train rides, and firm commitment that we will get through everything together.

1 Introduction

The human heart operates as a rhythmic pump, which is triggered to generate mechanical work by an electrical event, the action potential. Cardiovascular diseases are the leading causes of death in the United States[1]. Some of these deaths are due to mechanical dysfunction (when the heart fails as a pump, contributing to 650,000 deaths per year[1]) while others originate from electrical abnormalities (due to inconsistencies in rate and/or rhythm called arrhythmias, contributing to 480,000 deaths per year[1]). Clinical interventions for heart failure over the last fifty years have focused on pharmacologic and surgical approaches, but little improvements have been found in survival [1]. The inadequacy of available therapies has prompted recent investigations into the potential therapeutic use of stem cells. Although these stem cell therapies show promise, their interpretation has been hampered by an inability to define their location after delivery *in vivo* and determine their fate. The work in this dissertation is focused on overcoming this technical barrier by developing a novel stem cell tracking technique.

When the sinus node—the primary pacemaker of the heart—fails (sick sinus syndrome) or when conduction from the atrium to the ventricle is impeded (A-V block), an electronic pacemaker is often implanted. These pacemakers must be continuously monitored and their batteries and leads must be periodically replaced; thus, although they can prevent sudden cardiac death in the event of an acute arrhythmia, these devices are not a cure[2]. Previous studies from our laboratory have demonstrated that hMSCs transfected with the HCN2 gene—a member of the gene family responsible for pacemaker activity in the heart—can be injected into the canine heart to function as artificial pacing "nodes"[3]. Although these initial studies have shown functional recovery and the engraftment of hMSCs, no three-dimensional picture of the delivered stem cells has been attempted. A complete understanding of the spatial organization of an exogenous stem cell "node" is necessary in order to understand the biophysical mechanism driving biological pacemaking.

When cardiomyocytes die, the number of contracting units decreases. Traditional dogma describes myocardium as post-mitotic[4], and therefore research has recently focused on replacing defunct tissue with a novel substrates (i.e. Urinary Bladder Matrix, UBM, for review see [5]). Our laboratory has developed a protocol for *ex vivo* differentiation of hMSCs into "cardiogenic cells" committed to a cardiac lineage. These cells have been implanted into the canine ventricle on a UBM patch and contribute towards functional regeneration of damaged myocardium[6]. However, to determine whether these cells contribute to the repair process by becoming myocytes requires tracking the fate of the delivered cells.

Both applications of hMSCs—for restoration of contractile and electrical function—require the ability to track therapeutic cells after delivery to animal models *in vivo*. Questions of efficacy and safety for cell therapies can only be addressed by completely and unambiguously identifying delivered cells in the host tissue and determining their fate. This has been a major challenge in our laboratory and others (for review see [7-9]). The work herein examines the potential of quantum dot nanoparticles (QDs) to serve as a tracking vehicle. It will be demonstrated that: **Quantum dot (QD) nanoparticles can be used as a long-term vital labeling agent to track the location and fate of hMSCs *in vitro* and *in vivo*.**

2 Background

2.1 Epidemiology and pathology of heart disease

Cardiovascular diseases underlie 1 in every 2.7 deaths in the United States and have been the number one killer of Americans for the past 85 years[1]. When blood flow to a region of the heart is compromised, that tissue is deprived of essential nutrients and cell death ensues. Heart cells, unlike most other cells in the body, have traditionally been considered amitotic. This suggests that once these cells—responsible for the contractile and electrical behavior of the heart—are lost, they can never be replaced. Studies have shown that 70-80% of people under age 65 who have heart failure will die within 8 years[1].

Mechanical heart failure arises when large numbers of contractile cells die and a region of the ventricle fails as a pump. Such an event typically occurs as a consequence of atherosclerosis. This disease has a slow progression, leading to deposition of cholesterol plaques on the artery walls that can hinder blood flow. Eventually, the lumen of the vessel reaches a critical minimum diameter, wherein downstream vessels are not adequately filled and the cells they feed are starved. Treatment approaches for heart failure are first and foremost preventive. Patients are directed to use diet and exercise as a means of lowering LDL cholesterol levels in the blood and keeping blood pressure levels in check. When these methods fail, cholesterol-lowering drugs (i.e. statins) and anti-hypertensives (i.e. diuretics or in advanced disease, β-blockers) are administered. When heart failure appears inevitable, some patients undergo invasive procedures such as angioplasty or coronary bypass surgery to re-perfuse the jeopardized tissue. As a last resort, other surgical interventions that can be applied include implanting of ventricular assist devices (VADs), or total heart transplantation.

Much as dying contractile myocytes can disrupt mechanical function of the heart, so too can dying pacing cells disturb electrical behavior. Disorders of heart rhythm such as ventricular fibrillation arise when the primary pacing cells (the sinus node) fail to maintain the electrical synchrony of the heart. Patients suffering from fibrillation or tachycardia may have an electronic pacemaker implanted into the heart or they may sometimes undergo a procedure known as radio ablation to permanently destroy re-entrant paths in the conduction pathway.

In the cases of both mechanical and electrical heart failure, treatment approaches involve prevention and palliation, but do not attempt to cure the underlying pathology. Within the last decade, however, dogma has shifted and myocardium is no longer viewed as a static tissue incapable of self-repair[4]. Stem cells have shown promise for restoration of contractile[10-12] and pacing[3, 13, 14] functions in the heart and may prompt a new wave of treatments for cardiovascular diseases.

2.2 Stem cells for cardiovascular repair and regeneration

Stem cells are found in mammals in both embryos and adult tissue. These cells have two important characteristics: they can remain undifferentiated cells capable of self-renewal, or they can differentiate[15]. Embryonic stem cells, derived from the inner cell mass of a blastocyst are pluripotent, meaning they can differentiate into any cell type of

the three germ layers. Adult stem cells, however, lack this pluripotentiality but are considered multipotent because an adult stem cell can differentiate into a cell type of the same germ layer from which its host tissue was derived. For example, a bone marrow-derived mesenchymal stem cell can theoretically become any mesodermal cell type, because the bone marrow is a mesodermal tissue. In addition to the bone marrow, adult stem cells have been found to reside in many organs, including the brain, liver and skeletal muscle, where they function to repair damaged tissue (see [16] for review). Recently, stem cells have been identified in adult hearts, suggesting that they might be targets for endogenous repair of myocardium[17-19].

The role of stem cells for therapeutic repair is highlighted in cancers of the blood. For example, the principal defect involved in one form of leukemia is aberrant growth of a specific subset of white blood cells known as T-cells[20]. These cells are derived from multipotent progenitor stem cells in the bone marrow. Therefore, clinical intervention for leukemia relies on chemotherapy to destroy a sick patient's diseased white cells followed by bone marrow transplantation to introduce new, healthy stem cells. These stem cells self-renew in the host and from these transplanted cells, multiple lineages of healthy white blood cells can be derived[20].

If resident stem cells are identified in skin, liver, brain and muscle and have been linked to physiologic repair and regeneration, might stem cells also be used to repair myocardium? The heart differs from these other organs because its functional cells have traditionally been regarded as amitotic[4]. Investigations are already underway to regenerate damaged heart tissue with stem cells based on models of endogenous and exogenous repair.

2.3 Human mesenchymal stem cells for cardiovascular repair

We have used human mesenchymal stem cells (hMSCs) as a cellular platform for myocardial repair and regeneration. hMSCs are a subfraction of bone marrow cells (~0.001-0.01% of nucleated cells)[21] that have recently gained attention for use in cellular therapies. Some of the unique traits that make them attractive for this purpose are that they are: (1) easy to harvest and expand *ex vivo*, (2) are genetically stable, (3) have reproducible characteristic and (4) appear to be immunologically tolerated when delivered to an allogenic recipient[21]. This last feature is especially important because it will facilitate marketability as a clinical therapy.

Clinical trials using hMSCs [11, 22] and other bone marrow-derived cells[23] to repair myocardial tissue are already underway. Functional outcomes of these studies are inconclusive and the authors repeatedly advocate the need to select and expand hMSCs *ex vivo* prior to delivery. In their patent application, Pittenger, *et al*, [24] claim that hMSCs exert reparative effects *in vivo* by differentiation into functional myocytes. Challenging this idea, Hare recently reported that hMSCs repair myocardium by paracrine effects, possibly via induction of endogenous stem cell niches[25]. Our laboratory is presently trying to address these questions.

2.4 Ongoing repair studies in our laboratory involving hMSCs

In our laboratory, we are interested in inducing cardiac regeneration using hMSCs that are partially committed towards becoming cardiac myocytes. We have previously developed an *in vitro* method to partially differentiate hMSCs along a cardiac lineage to

generate a set of cardiogenic cells that are capable of self-renewal and upregulate several cardiac-specific markers *in vitro*[6]. We deliver these cells *in vivo* via an extracellular matrix patch and have measured functional improvements in the patch region eight weeks after implantation[6]. This repair may be due to (1) terminal differentiation of our cardiogenic cells into mature functional myocytes *in situ*, paracrine factors that (2) induce neighboring myocytes to re-enter the cell cycle or that (3) recruit host bone-marrow-derived stem cells to populate the region and participate in regeneration through further signaling or via transdifferentation, or (4) by induction of resident cardiac stem cells to proliferate and/or differentiate. In order to discriminate among these mechanisms for the observed repair we must characterize the fate of stem cells after delivery *in vivo*; to do this it is necessary to unambiguously identify them amidst all other host cells.

We are also using hMSCs to repair the electrical behavior of damaged myocardium. For these studies, the stem cells are transfected via electroporation to express the murine HCN2 gene (a key pacemaker gene). The genetically modified cells couple with host myocytes after injection into the canine heart, and serve as a backup biological pacemaker once heart block is induced[3]. Of critical importance in these studies is to understand the spatial distribution of the stem cells *in vivo*, and any changes in this distribution over time. Because the transfected cells are electrically active, wandering cells could potentially induce fatal arrhythmias. Thus, a cell labeling method is required that permits tracking and defining the spatial configuration of all of the stem cells after delivery *in vivo*.

2.5 Challenges of tracking stem cells in myocardium

Tracking cells in the heart is especially challenging because of the high levels of endogenous fluorescence in the myocardium, a property know as autofluorescence. There are a host of biochemical sources for autofluorescence in mammalian tissue that can be excited by light in the 360-480-nm wavelength range. These chemicals are both green and red emitters of light and include nicotinamide-adenine dinucleotide phosphate (NAD(P)H, emitting at ~509-nm), lipofuscins (emitting at 540-560-nm and rampant in post-mitotic cells such as myocytes), and collagen and elastin (emitting at >515-nm)[26]. Emission spectra of all of these substances are broad and overlap with many of the fluorescent reagents that are traditionally used to label cells. Furthermore, since damaged myocardium contains inflammatory cells with high levels of oxidative enzymes such as NAD(P)H and scar tissue is comprised of collagen, autofluorescence becomes even more significant under these conditions[27].

Existing techniques for tracking cells include (a) transfecting cells *in vitro* with either fluorescent (i.e. GFP)[3] or non-fluorescent (i.e. β-galactosidase) proteins[28], (b) employing fluorescence *in situ* hybridization (FISH) to identify delivered cells by their unique chromosomal content (i.e, male cells delivered to a female host)[29], (c) using species-specific surface markers to identify delivered cells in a xenographic host[3], (d) using commercially available fluorescent dyes to label cell cytoplasm[30] or nuclei[31], or more recently (e) labeling cells with inorganic particles (i.e. Feridex)[30, 32, 33] or radiotracers[30, 34-36]. The above can be grouped into two categories: those techniques requiring secondary staining to visualize cells in histologic sections (a-c) and those not requiring secondary staining (d and e). Although each of these approaches has advantages, they have generally focused on identifying the location and fate of a small

minority of the delivered cells or produced low resolution representations of *in vivo* stem cell distribution.

Within the first category of techniques, transfection is inefficient and cannot label 100% of the cells. Loading cells with exogenous DNA also requires use of viruses, lipofectamine vehicle or electroporation; each of these processes causes some cell death. Immunostaining—employed when tracking cells with FISH or by surface markers—often generates false positives[27] and interpretation of staining outcomes can be difficult in the absence of strict controls. Stem cells are also dynamic, and may change their surface marker expression over time if they differentiate *in vivo*. Furthermore, staining results and image features are typically heterogenous across a given tissue section and between sections, making it important to carefully sample the specimens and making quantitation difficult. In summary, immunostaining is a low-throughput process that is not practical to account for all delivered cells.

The second category of cell tracking approaches—those not requiring secondary staining—represents a potentially higher-throughput avenue to identifying delivered cells. Fluorescent dyes, however, fail to demonstrate any advantage over other techniques since they must be taken up via lipid vehicles, are only retained for short periods of time, and are prone to photobleaching when imaged[37]. They also have narrow excitation spectra and their emission profiles have long tails into the red range (spectral crosstalk), making it a challenge to identify multiple probes simultaneously[38]. The emission spectra of fluorescent dyes also overlap with those of host tissue autofluorescence. In the cardiac milieu, for example, both normal and damaged myocardium emits autofluorescence that can easily be misinterpreted as exogenous fluorescent cells. This phenomenon occurs in almost the entire UV range[26, 27]. Some groups have labeled cells with the nuclear dye DAPI[30, 31] but this agent intercalates into DNA and can therefore interfere with normal cell function[37].

Recently, others have loaded stem cells with magnetic nanoparticles (superparamagnetic iron oxide, SPIO)[30] or radiotracers[36] and imaged delivered cells *in vivo* with MRI or PET scanning. This offers the advantage of identifying clusters of labeled cells non-invasively, but does not afford single-cell resolution. SPIO-loaded cells can be identified in histologic sections only by secondary staining techniques (i.e. Prussian blue reaction).

None of the existing tracking techniques offers the ability to unequivocally identify delivered cells *in vivo* with single-cell resolution using relatively high-throughput approaches (i.e. no secondary staining).

The qualities of an ideal agent for tracking stem cells have been outlined by Frangioni and Hajjar[7] and include the criteria that the agent (a) be biocompatible, safe and non-toxic; (b) not require any genetic modification or perturbation to the stem cell; (c) permit single cell detection at any anatomic location; (d) allow quantification of cell number; (e) have minimal or no dilution with cell division; (f) have minimal or no transfer to non-stem cells; (g) permit non-invasive imaging in the living subject over months to years and (h) require no injectable contrast agent for visualization. We additionally propose that the agent must (i) be detectable above autofluorescence.

We have investigated the use of quantum dots as vital labels for long term stem cell tracking *in vivo* because they appear to represent a novel solution to many of the challenges of stem cell tracking and satisfy most of the criteria outlined above.

2.6 Special properties of quantum dots

Quantum dots (QDs) are semiconductor nanoparticles that were discovered in the early 1980's in the laboratories of Louis Brus at Bell Laboratories and of Alexander Efros and A.I. Ekimov of the Yoffe Institute in St. Petersburg in the former Soviet Union. Semiconductors are composed of elements in the II-VI, III-V, or IV-VI columns of the periodic table. On the macroscopic scale, these materials are important constituents of modern electronic devices because their conductivity can be altered by an external stimulus. As nanoparticles, however, their quantum properties change dramatically such that energy levels are no longer closely spaced and therefore no longer considered continuous. Discrete energy levels establish a scenario called quantum confinement that confers unique absorptive and emissive behavior onto the fluorescent quantum dots.

The semiconductor at the core of a quantum dot is responsible for the impressive optical properties that will be discussed below. Several years after Brus' work at Bell Laboratories, two of his colleagues at Bell, Dr. Moungi Bawendi and Dr. Paul Alivisatos found that coating the dots with a passivating inorganic shell further stabilized their fluorescence; they also developed methods to make QDs water soluble[38]. Thus, the QDs that are used for biological applications consist of a cadmium selenide or cadmium tellurium semiconductor core, a zinc sulfide inner shell and an outer polymer coating. The result is a water-soluble particle 13-15nm in diameter (Figure 2.1.1a).

Similar to organic fluorophores like fluorescein, QDs absorb photons of light of one wavelength and emit light of a different wavelength. Traditional fluorophores use absorbed energy to transfer electrons to excited states and energy is released (in the form of fluorescent light) when these electrons return to their resting states. When electrons move to different energy levels in QDs, they behave analogously, generating electron holes called excitons. The quantum system of excitons makes QD fluorescence much brighter and more photostable (less prone to photobleaching) than traditional fluorophores that use conjugated double bond systems of energy transfer. The energy state of an exciton dictates the wavelength of light emitted by a particular QD after excitation. QDs have a unique property known as tunability, wherein the physical size of the QD determines the wavelength of emitted light. Smaller dots emit blue fluorescent light and as the core size of the dots increases, emitted light becomes redder. Another important feature that distinguishes QDs from conventional fluorescent dyes is the large distance between the wavelength of excitation and emission light (Figure 2.1.1b). This energy difference, known as the Stokes' shift, means that QDs can be excited by ultraviolet light at a wavelength much lower than the peak emission wavelength. In fact, QDs can be excited by any wavelength lower than their emission wavelength. Thus, both excitation of the particles and collection of emitted light are very efficient processes.

These special characteristics of QDs make them well suited for use in biological imaging, specifically in the highly autofluorescent milieu of the myocardium. Because of the large Stokes' shift, there is practically no overlap between absorption and emission spectra, facilitating collection of QD-specific emitted light. Tissue can be excited by light that's less likely to induce autofluorescence. Also, since autofluorescent emission tends to be more significant in the green range, red QDs can be preferentially used. Their extreme brightness allows for very low exposure times when imaging QDs in biological tissues, decreasing the likelihood of simultaneously collecting autofluorescence. Finally,

as multiplex imaging of several markers is often desirable in biology, the broad excitation spectrum of QDs allows simultaneous detection of different sized QDs by the same incident light (Figure 2.1.1c).

2.7 Quantum dots for biological applications

Two landmark studies appeared in *Science* in September of 1998, documenting the first biological uses for QDs[38, 39]. Since then, several groups have emerged with novel applications. Dubertret, *et al*[40] reported the encapsulation of QDs within micelle-forming hydrophilic polymer-grafted lipids and delivered them via microinjection to single cells of Xenopus embryos. Major findings from this study were that only the originally injected cells and their progeny retained QDs, labeled cells showed no signs of toxicity, all embryonic cell types were able to arise from labeled cells, the QD fluorescence was detectable above high levels of autofluorescence and most importantly, QDs were biocompatible. This group was also the first to report the pitfall that intracellular QDs tend to aggregate around the nucleus over time[40]. A similar study published in 2005 demonstrated the use of QDs as lineage tracers by microinjecting them into single cells of zebrafish embryos. Here it was shown that the dots were nontoxic, retained their emission spectra regardless of microenvironment, could be induced to avoid perinuclear aggregation by surface modification with streptavidin, did not pass through gap junctions, and could be imaged in aldehyde-fixed tissue[41]. Both of these studies showed that the presence of intracellular QDs did not affect proliferation or differentiation of cells nor did they preclude formation of a fully-grown organism.

In 2003, two articles appeared in *Nature Biotechnology* demonstrating that populations of cells could be labeled with QDs. Jaiswal, *et al*, reported a receptor-mediated and generalizable endocytotic method for introducing QDs into the intracellular space for live cell imaging[42]. Unfortunately, the images in this paper again revealed the problem of perinuclear aggregation. Wu, *et al*, highlighted the ability of QDs for use in multiplex immunostaining of fixed cells[43]. Others have compared loading populations of cells via commonly used approaches including receptor-mediated transfection with a host of proteins[44-48], lipid-mediated transfection and electroporation[49]. While both lipid-mediated transfection and electroporation have the added problem of causing some degree of cell death, none of the approaches reported to date have uniformly and efficiently loaded populations of cells and all have resulted in perinuclear aggregation.

Figure 2.1.1. Anatomy and behavior of quantum dots
(a) The QD used in these experiments consists of a CdSe semiconductor core (red) that confers its unique fluorescent properties. However, this material has a reactive surface that is prone to degradation and must be passivated by a ZnS shell (gray). This unit must be further coated with a polymer (blue) for solubility in water and biocompatibility. The final size of the QD is approximately 13-15nm in diameter. QDs have broad excitation bands and narrow emission spectra. (b) The wavelength of light emitted by a QD is dependent on its physical size; QDs of different core sizes can be excited by the same wavelength of light (blue arrows, top) but emit unique colors of fluorescent light. (c) The peak of emitted light is shifted well to the right of the excitation wavelength. This property, know as the Stokes' shift, is much larger for QDs (left) than traditional fluorophores such as fluorescein (right). This makes both excitation and emission very efficient and is one of the ways in which QDs mitigate the effects of autofluorescence. Images in (a) and (c) adapted and image (b) reproduced from Qdot Corporation http://www.qdots.com.

a

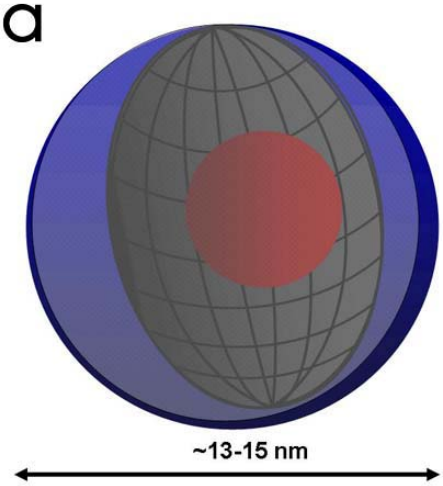
~13-15 nm

b

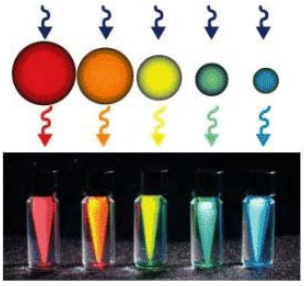

c

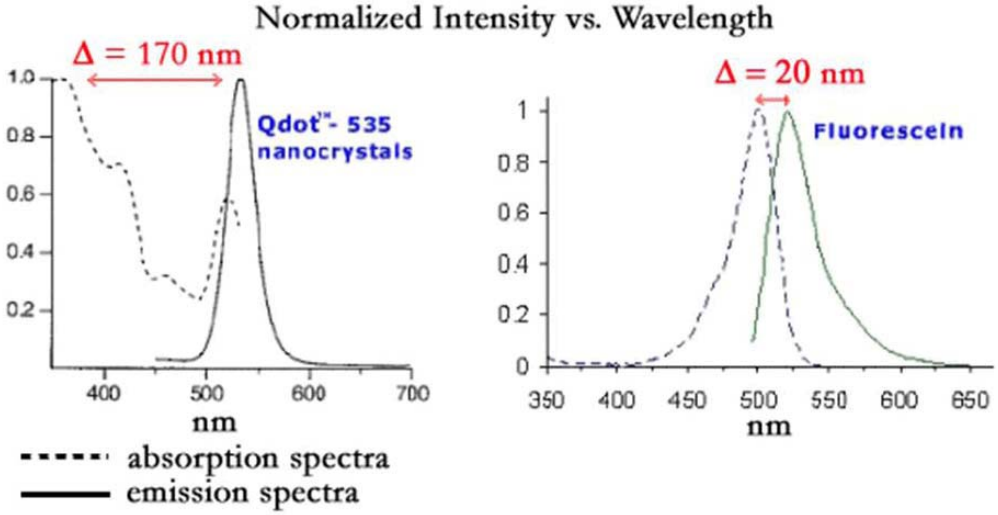
Normalized Intensity vs. Wavelength
Δ = 170 nm
Qdot™- 535 nanocrystals
1.0
0.8
0.6
0.4
0.2
400
500
600
700
nm
absorption spectra
emission spectra
Δ = 20 nm
Fluorescein
1
0.8
0.6
0.4
0.2
0
350
400
450
500
550
600
650
nm

3 Overview of Research Findings

This dissertation describes a novel method of loading human mesenchymal stem cells (hMSCs) with naked quantum dots (QDs) via passive endocytosis. Efficient and complete loading depends on the size and surface charge of the dots as well as the composition of the incubation medium. The location and fate of QD-labeled stem cells can be tracked *in vitro* for at least 6 weeks (and at least 5 cell divisions) and *in vivo* for at least 8 weeks. The major research findings described herein are summarized below.

Chapter 4.1. A method for uniformly labeling hMSCs with QDs has been developed and validated. QDs are retained by dividing cells over multiple divisions and cells are detectable for at least 6 weeks *in vitro*. The dots are not transferred to neighboring cells. QDs do not affect stem cell proliferation or differentiation, and differentiated cells retain the label.

Chapter 4.2. QDs are used to track hMSC location after injection into myocardium. The complete distribution of a stem cell "node" has been reconstructed in 3-D.

Chapter 4.3. QDs are used to track hMSC fate 8 weeks after delivery to canine myocardium on an extracellular matrix patch. Differentiation of QD-labeled hMSCs into endothelial and myocyte fates has been observed.

Chapter 4.4. μCT scanning to visualize QD-hMSCs is tested. The results suggest that QDs can be used to visualize hMSCs non-invasively in living animals.

4 Research Findings

4.1 Quantum dot (QD) nanoparticles as a long-term vital labeling agent to track hMSCs in vitro.

4.1.1 Introduction

This chapter addresses a series of *in vitro* experiments that were designed to validate the use of quantum dot (QD) semiconductor nanoparticles for tracking stem cells *in vitro* and *in vivo*. The first challenge in developing a novel cell tracking method is to identify a suitable labeling agent. In Chapter 2, we discussed the virtue of using QDs for this purpose. The experiments described in this chapter outline a series of trials to generate a method for uniformly loading human mesenchymal stem cells (hMSCs) with QDs. The starting points for these attempts were based on traditional methods for transfecting cells with exogenous genes (i.e. electroporation, lipofection) and recently found by other investigators to be useful for labeling cells with QDs[42, 45-48, 50].

Since the late 1990's many studies have touted the benefits of using QDs for biological applications. The earliest of these studies relied on custom-fabricated QDs[38, 39], but more recently, QDs with high quantum yields, high stability and uniform properties (monodispersity) have come to market. These QDs are available in a variety of colors (with varying semiconductor core sizes) and having various surface conjugations. Invitrogen sells QDs that emit fluorescent light in the green to near infrared range and for our experiments we tested cell labeling with green (525-nm), red (655-nm) and near infrared QDs (705nm and 800nm). Another consideration was the surface charge characteristics of the dots; we tested QD loading with dots having carboxylated (negatively-charged) surfaces and dots with additional PEGylation amino conjugations (positively-charged) at the surface.

For a cell labeling method to be optimal for any *in vitro* or *in vivo* stem cell tracking purposes it must satisfy the following four criteria: (a) uniform loading of the majority of a population of cells; (b) sustained intracellular distribution of label over extended time periods; (c) no transfer of label to neighboring cells; (d) no effect on cell viability. In addition, to track cell fate a fifth requirement is necessary: (e) no effect on differentiation capacity. The experiments described below summarize the data available to support evidence that we have satisfied these criteria.

4.1.2 Methods

Cell culture

Human mesenchymal stem cells (hMSCs) were obtained from Clonetics/BioWhittaker (Walkersville, MD) and early passages (p3-p7) were used for all experiments. Cells were grown on polystyrene tissue culture dishes and maintained at 37^{o}C in humidified 5% CO_2 in Mesenchymal Stem Cell Growth Media supplemented with L-glutamine, penicillin and serum (MSCGM BulletKit, Cambrex). Cells were re-plated for passaging once every two weeks. For isolation of canine cardiac myocytes, adult mongrel dogs were intravenously injected with 80mg/kg body weight sodium

pentobarbital according to an approved protocol. Hearts were then removed and placed in a cold, high-potassium Tyrode solution [51]. Myocytes were isolated using a modified Langendorff system with digestion via Worthington type II collagenase [52], cultured onto laminin-coated glass coverslips and maintained in Dulbecco's Modified Eagle Medium (DMEM) with 1% penicillin/streptomycin. Human umbilical vein endothelial cells (HUVECs) were obtained from Cambrex and cultured in their Endothelial Growth Media.

Quantum dot loading

Three approaches were used for loading hMSCs with QDs. First, a nucleofection protocol was followed to electroporate approximately $5x10^5$ hMSCs in 8.2 nM QDs (Qdot 655 ITK Carboxyl Quantum Dots, Invitrogen Cat. No. Q21321MP) solution (supplemented Human MSC Nucleofector Solution, Amaxa Biosystems, Cat. No. VPE-1001). After electroporation, cells were re-plated in complete MSCGM media onto polystyrene tissue culture dishes. Second, a commercially available kit was used to load the cells with QDs via a carrier protein (Qtracker 655 Cell Labeling Kit, Invitrogen Cat. No. Q25021MP). Briefly, 10nM of labeling solution was prepared according to kit directions, and approximately 0.2mL was added to a 100-mm polystyrene tissue culture dish containing roughly $5x10^5$ cells. The cells were incubated at 37^oC for 45-60 minutes, after which time they were washed twice with complete MSCGM. The third (and optimal) loading technique will be referred to as passive loading. Cells were grown to 85% confluence on polystyrene tissue culture dishes. An 8.2nM solution of 655 ITK Carboxyl QDs was prepared in complete MSCGM and vortexed for 60 seconds. Cells were washed once in phosphate-buffered saline (PBS) and incubated in the QD solution for up to 24 hours at 37^oC.

Quantum dot validation and mechanistic experiments

After the incubation period, cells were washed twice in PBS and fresh MSCGM was replaced. Loading efficiency was analyzed visually from a set of images of QD-hMSCs as well as by flow cytometry. In the first method, 181 cells from four QD fluorescence and phase contrast overlay images were studied and identified as either QD positive or negative. Loading determination via flow cytometry was assessed using the following protocol: hMSCs were loaded with QDs for 24 hours as described above. After the loading period, cells were washed twice in PBS, trypsinized and resuspended in PBS with 5% FBS. Cells were then stained with 7-amino-actinomycin D (to determine viability) and subsequently analyzed using a LSR II true multiparameter flow cytometer analyzer (BD Biosciences with custom 655-nm filter). Two sets of QD-hMSCs (and unloaded hMSCs for control), each set containing a minimum of 15,000 cells, were analyzed. The intensity range for control cells was set such as to include at least 98% of the viable cells. The same technique was used to scan the QD-hMSCs and determinations of QD-positive status was based on viable cells in the intensity range above that set for control. To determine the degree of loading after repeated cell divisions, cells were passaged three times at 1:4 for a minimum of 5 divisions over 44 days. For one set of experiments intended to determine the mechanism of loading, hMSCs were passively exposed to QD incubation medium for 7 hours at either 4^oC or 37^oC. In another approach, cells were passively exposed to QD incubation medium for 12 hours either in MSCGM or 125μM colchicine (Sigma, Prod No C9754) in MSCGM.

To determine if canine cardiac myocytes (cCMs) would take up QDs, cultured myocytes were exposed to a passive loading protocol (8.2 nM QDs in DMEM supplemented with 20% FBS and 1% Penicillin/Streptomycin) for 24 hours or were incubated with mechanically lysed QD-hMSCs; in this second case, cCMs were incubated for up to 24 hours in DMEM to which the lysate from approximately 10^4 cells was added.

Viability assay

A population of hMSCs was evenly split for passaging and both dishes were grown to ~85% confluence. One dish was passively loaded with QDs as described above while the other received a media exchange. The following day (after 24 hours of loading), both dishes were washed and re-plated at equal concentrations into 12 wells each of a 96-well dish and cells were allowed to grow for 3 days. The mitochondrial dehydrogenase assay (MDA, KKBiomed) was carried out according to instructions provided by the company. The absorbance of each of the samples was measured at 595-nm using a Polarstar OPTIMA microplate reader (BMG Technologies).

Differentiation of QD-hMSCs

Induction was performed using adipogenic, osteogenic and chondrogenic kits available through Cambrex (Adipogenic Differentiation Medium, PT-3004; Osteogenic Differentiation Medium, PT-3002; Chondrogenic Differentiation Medium, PT-3003). All experiments were performed in triplicate on both QD-hMSCs and hMSCs.

For adipogenesis, labeled and unlabeled cells were plated at $2x10^4$ cells/cm^2 tissue culture surface area and fed every 2-3 days with MSCGM until cultures reached 100% confluence (5-13 days). Cells were fed on the following regime for a total of 3 cycles: 3 days with supplemented Adipogenic Induction Medium followed by 1-3 days with Adipogenic Maintenance Medium. Control hMSCs were fed with Adipogenic Maintenance Medium at all times. After the 3 cycles, all cells were cultured for another week in Adipogenic Maintenanc Medium. Cells were analyzed using light microscopy for characteristic lipid vacuole formation.

For osteogenesis, cells were plated at $3x10^3$ cells/cm^2 tissue culture surface area and cultured overnight in MSCGM. Cells were then fed with Osteogenesis Induction Medium with replacement media every 3-4 days for 2-3 weeks. Non-induced control cells were fed with MSCGM on the same schedule. Cells were analyzed using light microscopy for characteristic cobblestone appearance.

Finally, chondrogenesis was induced by pellet formation ($2.5x10^5$ cells/pellet), in Complete Chondrogenic Medium containing fresh TGF-β3. Pellets were formed with either 100% hMSCs, 100% QD-hMSCs or 50/50% hMSCs/QD-hMSCs. Pellets were fed every 2-3 days with fresh Complete Chondrogenic Medium for 21 days, after which time pellets were rinsed in PBS, fixed for 1 hour, cryoprotected in 30% sucrose and embedded for frozen sectioning. Serial 10μm histologic sections were stained with Hoescht and mounted in Cytoseal for QD visualization or analyzed for the presence of glycosaminoglycans using Safranin-O staining. Briefly, sections were stained in Weigert's iron hematoxylin for four minutes (hematoxylin and ferric chloride from Sigma-Aldrich, St. Louis, MO), destained in fresh acid alcohol, rinsed in tap water, stained in 0.02% aqueous fast green FCF (Sigma-Aldrich, St. Louis, MO) for three minutes, washed in 1% acetic acid (Sigma-Aldrich, St. Louis, MO) for 30 seconds, and

stained in 0.1% aqueous Safranin O (Sigma-Aldrich, St. Louis, MO) for five minutes. Sections were then dehydrated in increasing concentrations of ethanol, cleared in toluene and mounted with Permount (Fisher Scientific, Pittsburg, PA).

Visualization of QD-hMSCs

In vitro experiments were performed in polystyrene tissue culture dishes. For typical visualization, cells were re-plated onto CC2-coated glass chamber slides (Lab-Tek). Several hours after re-plating, slides were rinsed in PBS and then fixed in 4% paraformaldehyde (PFA) for 15 minutes. Slides were rinsed again in PBS for 5 minutes, and then incubated in 1μM Hoechst 33342 nuclear dye (Cambrex) for 20 minutes. They were then washed in PBS for 5 minutes and placed in dH_2O for 20-30 seconds. The slides were rinsed successively in 30%, 70%, 95% and 100% ethanol each for 30 seconds and then placed in 100% toluene for 30 seconds. Finally, slides were mounted in Cytoseal^{TM}60 (Electron Microscopy Systems) containing 1% triocytylphosphine (TOP, Sigma), with coverslips allowed to set overnight. Images were acquired on an inverted Zeiss Axiovert deconvolution microscope with AxioCam MRm CCD camera using a filter customized for 655-nm QD emission (Omega Optical, XF3305, excitation at approximately 420-nm); the DAPI filter set was used to visualize Hoecsht 33342-stained nuclei. For some images, z-stacks were obtained at multiple focal planes and subsequently deconvolved using AxioVision (ver 4.3, Carl Zeiss Vision, Germany). These stacks were then reassembled in ImageJ (ver 1.32j, NIH) into single 2-D images based on fluorescent pixels of maximum intensity at each section. All additional image processing was carried out using custom Matlab algorithms (Matlab 6.5 and 7.0, MathWorks, Natick, MA) or in ImageJ. For some experiments, imaging was performed on live cells using an Olympus inverted fluorescence microscope (Olympus IX51, DP70 camera) with GFP and Texas Red (for QD imaging) filter sets.

Computer algorithms

Custom algorithms (see Appendix) were designed and executed in Matlab 6.5 and 7.0 (MathWorks, Natick, MA). Images were obtained on the Zeiss Axiovert microscope using the 655-nm custom filter set described above, and then converted to jpg using Axiovision software (ver 4.3, Carl Zeiss Vision, Germany). For QD cluster analysis, QD fluorescence intensity images (63X) were obtained from cells at various time points after loading. Images were thresholded based on Otsu's method, to minimize the intraclass variance between black and white pixels. The individual binary image clusters were identified and their major axis lengths were determined in order to calculate cluster diameters. Corresponding nuclear images of Hoechst 33342 staining were used to compute the number of cells in the image fields. Finally, the number of QD clusters per cell was calculated for each time point.

Statistics

All data are listed as mean ± standard deviation. Data sets were compared by a Student's t-test with $p<0.05$ considered significant.

4.1.3 Results

QDs can be uniformly loaded into hMSCs

Several groups have attempted to load populations of cells with QDs via electroporation, receptor-mediated or non-specific endocytosis or using lipofection. We first tried loading hMSCs with 655-nm QDs using the commercially available QTracker kit (Invitrogen). This kit uses a proprietary protein to target positively-charged QDs into the cell via receptor-mediated endocytosis. Most of the hMSCs survived the loading procedure, but we were unable to uniformly label populations of cells (Figure 4.1.1a). Furthermore, we observed that after several days, intracellular QDs began to aggregate around the nucleus. These problems suggested that another approach would be desirable. Next, we tried loading both negatively-charged and positively-charged 655-nm QDs into hMSCS via electroporation. We observed that an appreciable number of cells were killed in the process. The electroporation also resulted in non-uniform, incomplete loading with eventual peri-nuclear aggregation. Finally, we exposed hMSCs to media containing either positively-charged or negatively-charged QDs of two different semiconductor core sizes (525-nm and 655-nm) with no additional biologic moieties on the surface (naked dots). When hMSCs were incubated in media containing negatively-charged 655-nm QDs, the cells uniformly and robustly picked up the label (Figure 4.1.1b-c). Furthermore, no peri-nuclear aggregation of dots was observed in these cells over several days (Figure 4.1.1d). All other combinations of dot surface charge and core size resulted in inadequate levels of loading. This *passive loading* approach was therefore the technique we chose to use to accomplish uniform loading.

QD-loaded hMSCs (QD-hMSCs) were imaged after loading for QD fluorescence and under brightfield conditions to acquire images of the cell borders and QD distribution. Based on 181 cells in four images, we estimated a >98% loading efficiency. To compliment this analysis, we performed flow cytometry on both QD-loaded and unloaded hMSCs to measure fluorescence intensities of single cells and characterize the populations. We determined based on these experiments that >96% of 31,000 cells analyzed were well loaded using the passive incubation technique (Figure 4.1.1e).

As a means of optimizing passive loading, we performed experiments in which hMSCs were exposed to the QD incubation medium for various durations (5 min, 10 min, 30 min, 1 hour, 3 hours, 7 hours, 12 hours, 24 hours, 48 hours). We imaged QD-hMSCs after these incubations and determined that low levels of loading were apparent after only 5 minutes of exposure, more significant loading was accomplished after several hours and cells were brightly labeled after 12 hours and longer (Figure 4.1.1g-i). We therefore chose incubation periods of 12-24 hours for most of our subsequent experiments.

To investigate the mechanism of uptake, we first hypothesized that dots were internalized by non-specific endocytosis. We therefore attempted passive loading of hMSCS in two conditions under which endocytosis should be decreased: 1) incubation at 4^{o}C and 2) incubation in the presence of the microtubule inhibitor colchicine. In both of these experiments, QD loading was dramatically reduced (Figure 4.1.1f), suggesting that passive loading relies on an endocytotic process.

A list of conditions under which loading was attempted and the respective outcomes is summarized in Table 4.1.1.

Diffuse cytoplasmic distribution of QDs is maintained over several weeks

QD-hMSCs were subpassaged over the course of 44 days, a period over which at least five cell divisions should have occurred. Images of QD-hMSCs were acquired at 2 days, 16 days and 44 days after loading (Figure 4.1.2a-c). Consistent with the notion that intracellular particles will distribute evenly to daughter cells during cell division, the absolute numbers of QD clusters per cell appeared to decrease over this period. However, the overall fluorescence intensities of the cells were well above the threshold of detection despite multiple divisions/dilutions. The intracellular QD cluster sizes were stable over this period ($0.84 \pm 0.11\mu m$, $0.91 \pm 0.21\mu m$, $0.94 \pm 0.13\mu m$, average cluster diameters for 2, 16 and 44 days after loading respectively) and the distribution remained cytoplasmically diffuse.

Intracellular QDs do not transfer to neighboring cells

We performed a series of experiments to identify any potential false positives that could arise later in our *in vivo* experiments. First, we queried whether QDs could transfer to adjacent cells. The only direct passage between the intracellular compartments of neighboring cells is the gap junction channel. Previous studies from our laboratory have demonstrated that hMSCs express connexins 43 and 40 and form functional gap junctions with other hMSCs and with cardiac myocytes when placed in close apposition[53]. This channel has a pore diameter of approximately 1-nm while a single QD has a minimum diameter of at least 10-nm. Despite this apparent physical disparity, we designed an experiment to investigate possible transfer of QDs from loaded to unloaded hMSCs. QD-hMSCs were cultured alongside hMSCs in which a plasmid encoding the expression of GFP was transfected. We looked for, but failed to find any occurance of red QDs inside GFP-positive cells in four separate experiments (Figure 4.1.3a).

Another potential source of false positives can occur if native myocytes have access to QDs after QD-hMSCs are delivered *in vivo*. One way this might occur is if delivered QD-hMSCs die and spill their contents into the extracellular space. We therefore exposed cultured adult canine myocytes to the lysis product from 100,000 mechanically ruptured QD-hMSCs for up to 1 week. No evidence of QD uptake by the myocytes was observed (Figure 4.1.3b).

Intracellular QDs do not affect hMSC proliferative capacity

To test the potential effect of intracellular QDs on the proliferative capacity of hMSCs, we performed a mitochondrial dehydrogenase assay (MDA, KKBiomed). This assay spectrophotometrically measures the production of the mitochondrial dehydrogenase enzyme, which is associated with cell viability, by its reaction with a colorimetric substrate 3-[4,5-dimethylthiazol-2-yl]-2,5-diphenyl tetrazolium bromide (MTT). We used the assay to compare proliferation between QD-loaded and unloaded hMSCs. No differences between the two groups were identified (0.1405 ± 0.0165 vs. 0.1186 ± 0.0230 respectively, N=12 per group, see Figure 4.1.4).

Intracellular QDs do not affect hMSC differentiation capacity

One possible function of stem cells is differentiation along specific lineages. If QDs are to be used for tracking stem cell fate then their presence must not affect the cells' capacity to differentiate. Furthermore, the label must be retained throughout the

differentiation process to enable identification of the derivatives of the original QD-hMSCs. QD-loaded and unloaded hMSCs were cultured under conditions of adipogenesis, osteogenesis or chondrogenesis. After 23 days of adipogenic induction, both unloaded and QD-loaded hMSCs showed similar levels of differentiation (44.9% and 40.4% area occupied by adipocytes respectively for fields of view shown in Figure 4.1.5a and b). Furthermore, terminally differentiated adipocytes originating from QD-loaded hMSCs retained the QD label (Figure 4.1.5c). Both unloaded and QD-loaded hMSCs responded to the osteogenic induction similarly (although it was not possible to quantify from the images because of over-confluence and difficulty discerning cell boundaries in the phase intensity images), with both groups of cells showing characteristic changes in morphology from spindle-shaped to cobblestone-shaped and tendency toward clustering by day 15 (Figure 4.1.5d and e respectively). Again, cobblestone-shaped osteocytes derived from QD-hMSCs still contained QDs at the end of the differentiation process (Figure 4.1.5f). Finally, pellets of hMSCs or QD-hMSCs exposed to chondrogenic conditions contained similar levels of proteoglycans as determined by Safranin O staining (Figure 4.1.5g and h respectively). Cells within the pellets formed from QD-hMSCs retained the QDs (Figure 4.1.5i). Because of quenching effects of the organic reagents on the QD fluorescence it was not possible to visualize co-localization of QDs and positive Safranin O staining. However, by imaging serial sections we identified overlapping QD-positive and proteoglycan-positive regions (Figure 4.1.5i).

4.1.4 Discussion

The experiments described above demonstrate that we have developed a novel method of labeling stem cells with QDs. Existing methods for QD loading rely on electroporation, lipofection or receptor-mediated uptake and all of these methods have pitfalls, including increased cell death and perinuclear aggregation of the dots[40-42, 44-48, 54]. These are undesirable outcomes since perinuclear aggregation may compromise cell viability. In order to track the progeny of an original population of cells, that population must be uniformly and completely labeled, with diffuse distribution of dots within the cytoplasm.

Interestingly, others have reported QD labeling with positively-charged dots (by virtue of their protein coating) and published images of labeled cells that reveal weak labeling and non-uniformity. Intuitively, one would expect positively-charged dots to be more attractive than negatively-charged dots to the cell membrane because of its negatively-charged glycocalyx and phospholipids. In fact, it is for this very reason that gene transfections are performed with positively-charged plasmids. However, in our hands, positively-charged dots gave the worst results and negatively-charged dots loaded efficiently and uniformly without mechanical perturbation to the cell.

We have shown that when loaded by our approach, millions of hMSCs can be uniformly labeled with QDs simultaneously in as little as 7 hours. The loading process is 96-98% efficient. QDs do not aggregate around the nucleus and the uniform distribution of QDs in the cytoplasm persists over at least 6 weeks *in vitro*. Such endurance of the label will enable long term *in vitro* studies for tracking the location and fate of hMSCs.

One example of a type of study that could use QDs for cell tracking is an investigation into the effects of co-culturing hMSCs with other cell types. hMSCs can

produce a host of signaling molecules that may be important for paracrine effects on other cell types. In a co-culture setup where the two cell types are morphologically indistinguishable, or when characteristic cell shapes change over time in culture, it is important to label at least one of the populations. QDs could be used to label hMSCs in such a configuration. Since we have demonstrated that QDs do not transfer to neighboring cells, only the originally labeled hMSCs and their progeny would contain the QDs in such an experiment and would be distinguishable from the other (unlabeled) cell type. Cells could be tracked in real time, without the need for fixation or immunostaining.

QDs may also be useful for tracking migration of hMSCs. Some investigators are interested in the types of substrates that are favored by hMSCs. For example, the cells may form tighter adhesions and preferentially proliferate on an organic extracellular matrix more readily than on glass. In an experiment to study this effect, the QD-hMSCs could be easily imaged through thick matrix materials (see Chapter 4.3) and tracked in real time.

hMSCs are also being studied for their ability to differentiate into cell types of mesodermal lineage. We have shown that the presence of QDs within the cytoplasm does not interfere with the ability of these cells to differentiate along adipogenic, osteogenic or chondrogenic lineages. We have also shown that terminally differentiated cells derived from QD-hMSCs do not lose the label in the differentiation process. Therefore, *in vitro* studies of hMSC fate could be facilitated by tracking with QDs. In one potential experiment, the cells might be co-cultured with a terminally differentiated cell (i.e. hepatocyte) to encourage differentiation (i.e. hepatogenesis) via paracrine effects[55]. At the end of these experiments, QD-hMSCs could be sorted from the terminally differentiated cells using fluorescence activated cell sorting (FACS).

Figure 4.1.1. Uniform loading of QDs into hMSCs
QD loading was achieved by lipid mediated uptake or passive incubation. Panels (a) and (b) show images of QD fluorescence (655-nm, red) with phase contrast overlays. (a) Using the lipid vehicle resulted in non-uniform cellular loading with perinuclear aggregation. (b) In contrast, passively incubating hMSCs in QD media results in nearly 100% loading with a pattern that extends to the cell borders. (c) The field in (b) is imaged for QD fluorescence without the phase overlay to demonstrate homogeniety and brightness. The intracellular QD cluster distribution is uniformly cytoplasmic (c,d) and largely excludes the nucleus (blue, Hoechst 33342 dye). (e) QD loading efficiency was analyzed using flow cytometry. The threshold for plain hMSCs (gray line) was set such that the intensity range encompassed at least 98% of the control cells (red arrow indicates upper bound of control range). QD-positive status was designated for all cells in the QD-hMSC sample having intensities above the range set for the control group. In both of two experiments, QD-positive cells (black line) were found in 96% of over 17,000 viable cells. (f) When colchicine-conditioned cells are incubated with colchicine-containing QD media, the uptake is dramatically reduced. The cells in panel (f, colchicine) and (f, inset, no colchicine) can be directly compared, as the incubation periods were identical and the cells were imaged using the same microscope and camera settings. (g-i) hMSCs continually take up QDs from the incubation media. Cells incubated in QD media for (g) 1, (h) 3, and (i) 24 hours are all imaged using the same microscope and camera settings. Images are grayscale for clarity. Because of the different levels of loading, the exposure time (380 ms) used to image all three samples is clearly too high for the 24-hour-incubated cells; most of the QD clusters in the image are overexposed. Scale bar a, b = 50 μm; Scale bar c = 100 μm; Scale bar on d, f-i = 25μm

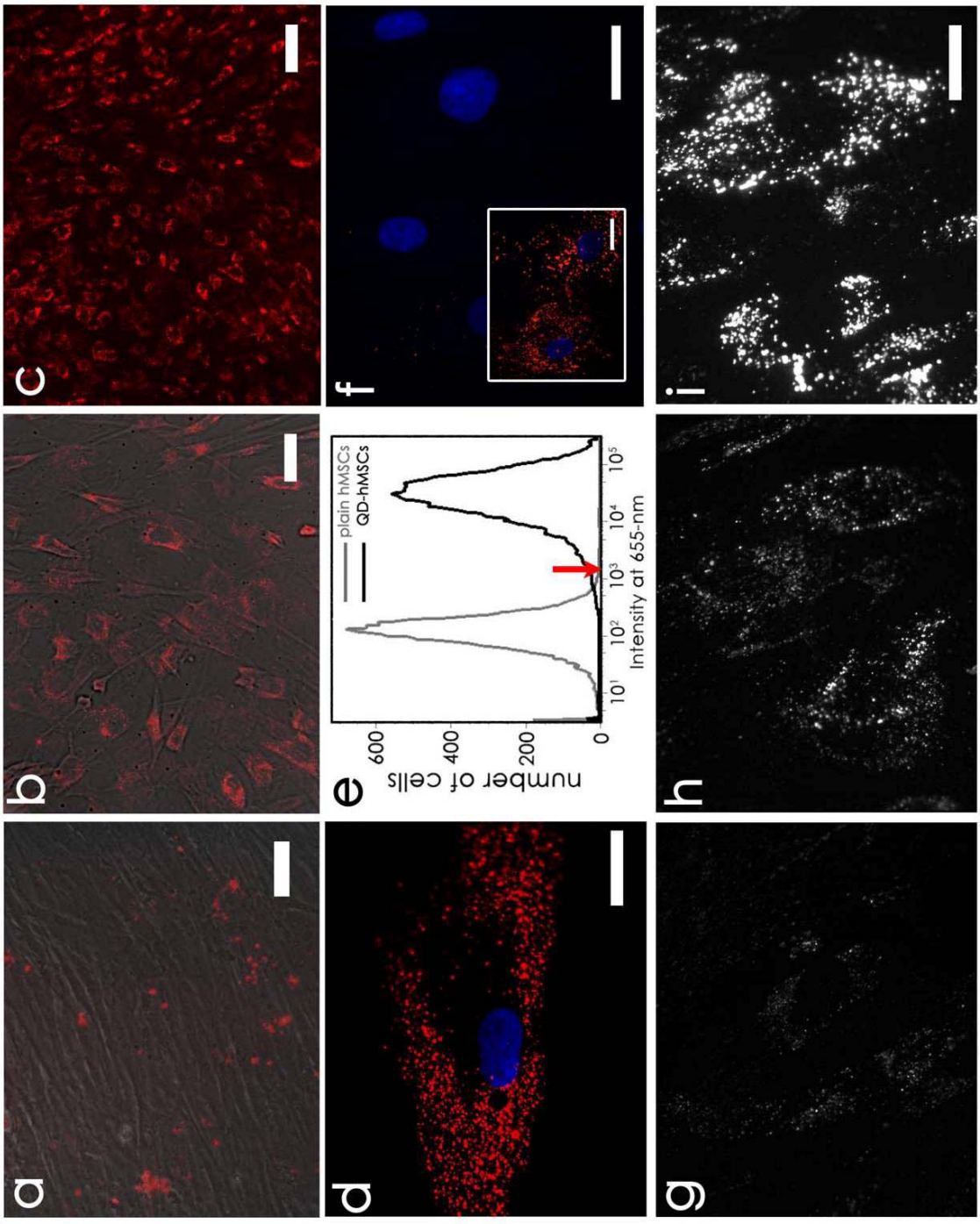
a
b
c
d
e
f
g
h
i
plain hMSCs
QD-hMSCs
number of cells
Intensity at 655-nm
0
200
400
600
10^1
10^2
10^3
10^4
10^5

Table 4.1.1. Summary of loading conditions
Attempts were made to load hMSCs by testing combinations of various parameters (listed at top). Negatively-charged dots had carboxylated surface derivitizations. Positively-charged dots had additional amino-PEGylation coatings on the surface. Some dots had additional streptavidin molecules conjugated to the polymer surface resulting in either net negatively-charged or neutral dots. Loading with QDs of larger core sizes (proportional to wavelengths of emission of 655-nm and 800-nm) was successful whereas loading with smaller dots (green, 525-nm) yielded much lower uptake. The most important variables for uniform and complete loading were: (1) surface charge, (2) core size, and (3) incubation media.

	Surface charge on dots			Additional conjugation	Emission wavelength (nm)			Method of loading			Media			Substrate	
outcome	+	0	-	Streptavidin	655	800	525	Passive incubation	Qtracker	Electroporation	Cambrex hMSC	DMEM	DMEM+ 10%FBS	Polystyrene	Glass
✓			•		•			•			•			•	
✓			•	•	•			•			•			•	
✗			•		•			•			•				•
✗			•		•			•				•		•	
✗			•		•			•					•	•	
✗					•				•		•			•	
✗			•		•					•	•			•	
✓			•	•		•		•			•			•	
✗		•		•		•		•			•			•	
✗		•		•	•			•			•			•	
✗	•				•			•			•			•	
✗			•				•	•			•			•	

Figure 4.1.2. QD brightness and uniform distribution is maintained over six weeks. QD-hMSCs were imaged for QD fluorescence at (a) 2 days, (b) 16 days and (c) 44 days after loading. Only the Hoechst (blue, nuclei) channels of these images have been post-processed to enhance contrast; QD channels (red) are displayed as imaged. As cells divide, they split their cytoplasmic contents to each daughter cell, diluting the ultimate concentration of QDs in progeny over time. Therefore, exposure times of excitation light need to be increased to optimally capture QD images of cells that have been through multiple divisions. Microscope and camera settings are the same for images (a) and (b), but in (c), cells are imaged for 655-nm (red) emission using triple the exposure time. The QDs in (a) are overexposed at this setting, with some clusters clearly saturating the image.
Scale bar a-c = 25 μm

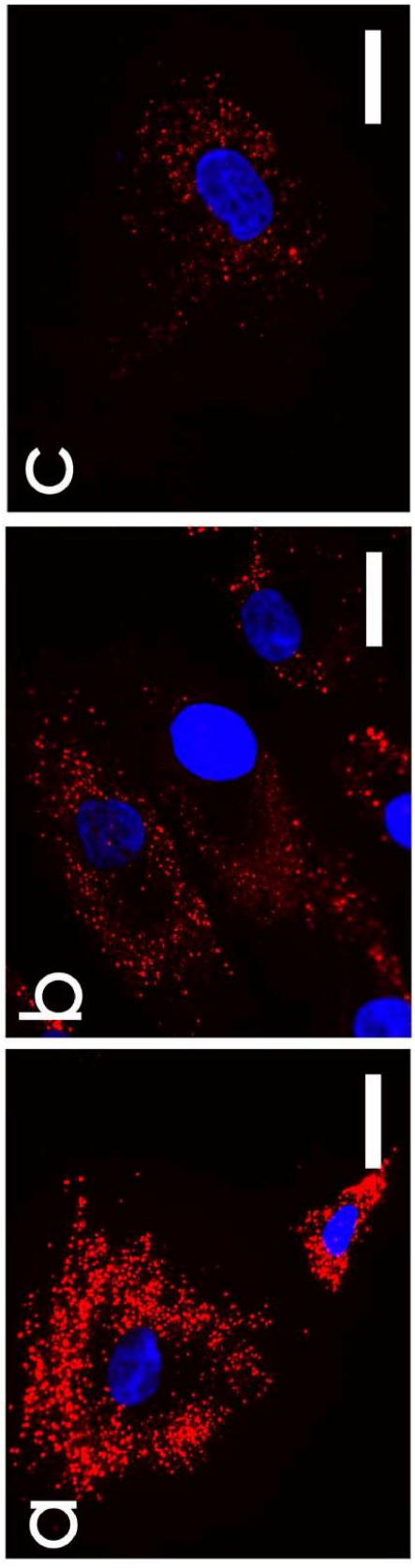
c
b
a

Figure 4.1.3. QDs do not transfer to neighboring cells
(a) Green (GFP transfected) and red (QD-loaded) hMSCs in direct apposition were imaged live to look for QD transfer to neighboring cells (colors have been enhanced for contrast). In a separate experiment, QD-hMSCs were mechanically lysed and then added to cultured canine myocytes for 24 hours. (b) A myocyte (right) sits near a live QD-hMSC that survived the lysis and attached to the coverslip. Floating QD clusters from the lysed cells are apparent in the media but were not internalized by the myocytes. Live cell images in (a) and (b) were acquired on an Olympus inverted fluorescence microscope using a GFP and a Texas Red filter, which does not optimally image the 655-nm QD signal.
Scale bar a, b = 50 μm

b

a

Figure 4.1.4. Intracellular QDs do not affect proliferation rate of hMSCs
QD-loaded and plain hMSCs proliferate similarly, as measured by a mitochondrial dehydrogenase assay (N=12).

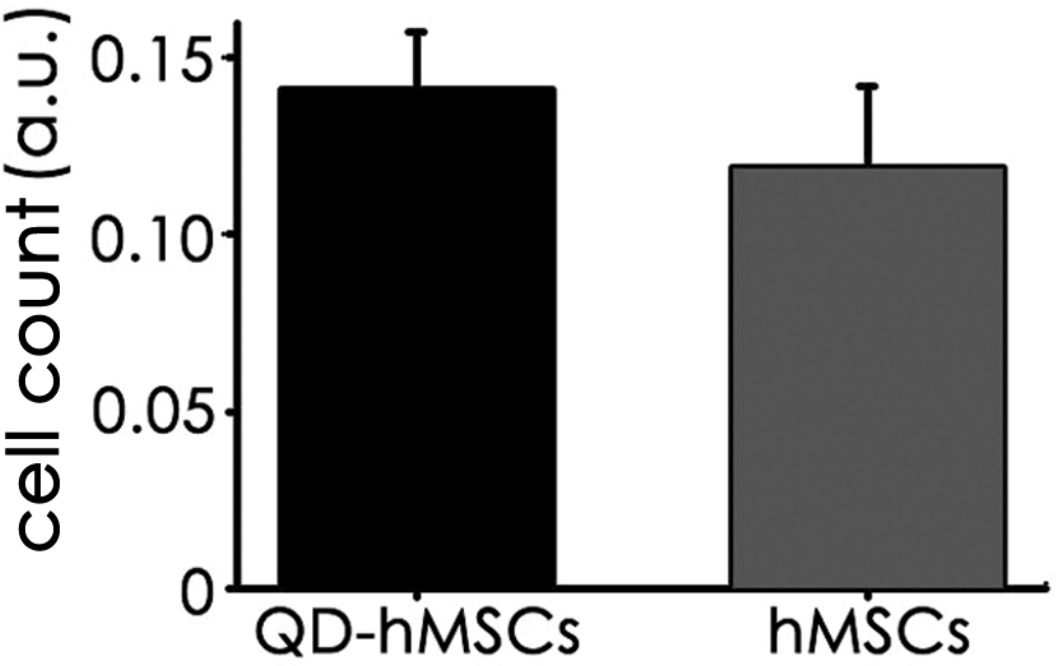
cell count (a.u.)
0.15
0.10
0.05
0
QD-hMSCs
hMSCs

Figure 4.1.5. QDs do not interfere with differentiation capacity of hMSCs *in vitro*
QD-hMSCs or unloaded hMSCs were induced to differentiate *in vitro* along adipogenic and osteogenic lineages. After the adipogenic induction period both (a) unloaded hMSCs and (b) QD-hMSCs displayed characteristic adipocyte morphology, with prominent lipid vacuoles. The percent of differentiated versus undifferentiated cells was similar between these two groups (44.9% in a; 40.4% in b). (c) At high power, adipocytes from the QD-hMSC group are seen with QDs (red fluorescence) interspersed between lipid vacuoles. After the osteogenic induction period both (d) unloaded hMSCs and (e) QD-hMSCs that were initially spindle-shaped adapted a more cobblestone-like morphology typical of osteocytes and tended to cluster on the dish. (f) At high power, a cobblestone-shaped osteocyte from the QD-hMSC group shows retention of the QD label (red) after the differentiation process. Histologic sections of cell pellets exposed to chondrogenic conditions were stained with Safranin O (proteoglycans, red; cytoplasm, gray-green; nuclei, black). (g) A section of a chondrogenic pellet formed from unloaded hMSCs stains positively for proteoglycans in the middle of the pellet. (h) A section of a chondrogenic pellet formed from QD-hMSCs is strongly positive for proteoglycans in the middle of the pellet. (i) A section serial to (h) is visualized for QD fluorescence and nuclei (Hoescht, blue); much of the QD-positive region overlaps with the proteoglycan-positive region seen in (h).
Scale bars on a,b,d,e,g,h,i = 200 μm
Scale bars on c,f = 50 μm

a
b
c
d
e
f
g
h
i

4.2 QD-loaded hMSCs are injected in vivo and reconstructed in 3-D to give a realistic view of the artificial "node."

4.2.1 Introduction

Having performed a set of *in vitro* experiments to validate the use of QDs for hMSC labeling and tracking, we moved on to explore *in vivo* applications for these labeled cells. hMSCs have recently gained attention for their potential use as biological pacemakers[3]. Genetically modified cells can be injected into the myocardium where they function as pacemaker "nodes." So far, only traditional cell tracking techniques have been used to identify small numbers of cells after injections in these experiments. These studies demonstrate the continued presence of the stem cells (via GFP detection and immunostaining for specific surface markers) but do not provide a picture of their three dimensional conformation. In the absence of this information, major concerns about safety and efficacy loom: do individual cells wander from the "node," and if so, will they compromise function or can they generate arrhythmogenic foci? What is the physical configuration of a stem cell "node" *in vivo* and does this shape change over time? This chapter describes a set of experiments performed in rats to characterize the 3-D spatial distribution of QD-hMSCs after myocardial injection. QD-hMSCs are also shown to retain their ability to be transfected and overexpress a key pacemaker gene.

4.2.2 Methods

Gene transfections

hMSCs were transfected with pIRES-EGFP (4 μg) or HCN2-pIRES-EGFP (4 μg) using the Amaxa biosystems nucleofection technique[3].

Patch clamping

Whole cell patch clamping was executed as previously described [3]. Patch electrode resistance was 4 to 6 MΩ. The pipette solution was filled with (in mM) K-aspartate 120, Mg-ATP 3, EGTA 10, and HEPES 5 (pH adjusted to 7.2 with KOH). The external solution contained (in mM) NaCl 137.7, KCl 5.4, NaOH 2.3, $CaCl_2$ 1.8, $MgCl_2$ 1, Glucose 10, and HEPES 5 (pH adjusted to 7.4 with NaOH). Recordings were made at room temperature.

Rat heart injections

QD-hMSCs were prepared as described in the previous chapter. 24 hours after QD incubation, cells were washed twice in PBS, trypsinized and re-suspended for a final cell concentration of approximately 10^5 cells/10μL in DMEM at 4^oC. The cell solution was stored on ice until injection. Rats (5-months-old, Charles River for normal rats; 12 weeks old Nude rats from Taconic, NIH Nude Outbred Rats, heterozygous, NIHRNU-T) were anesthetized with ketamine/xylazine intraperitoneally, intubated and maintained on inhaled isofluorane (1.5-2%) for the duration of the experiment. A left thoracotamy was performed at the 4^{th} or 5^{th} intercostal space. A 5-0 prolene suture was used to place a

superficial stitch in the epicardium as a fiducial marker. 10μL of cell solution or cell lysate was injected into the free left ventricular wall apical to the suture and then a small drop of surgical grade tissue adhesive (Nexaband, JA Webster) was applied over the injection site. The thorax was closed and rats were returned to their cages for either 1 hour or 1 day for whole cell injections, or either 1 hour or 1 week for the lysed QD-hMSC injections. Nude rats also received analgesic and antibiotics (baytril, 10mg/kg SC; ketorolac, 2-4 mg/kg). Euthanasia was performed either in a CO_2 chamber or by administering pentobarbital (100 mg/kg body weight injected intraperitoneally) and removing the heart.

Preparation of tissue samples

Immediately after explantation, tissue samples were rinsed in isotonic saline and then fixed in 4% PFA for 24 hours. After fixation, tissue was cryopreserved in an isotonic 30% sucrose solution for at least 24 hours. Gross photographs were obtained of tissue samples with sutures *in situ* to identify the cell delivery zone (either patch borders or injection site). After suture removal, tissue was embedded in freezing matrix (Jung tissue embedding matrix, Leica) and stored at -20^{o}C. 10-μm tissue sections were cut on a cryotome, transferred to Suprafrost glass slides and stored at -20^{o}C. Slides were either imaged without mounting, or stained with Hoechst 33342 dye and mounted as described in the previous chapter.

Computer algorithms

Custom algorithms (see Appendix) were designed and executed in Matlab 6.5 and 7.0 (MathWorks, Natick, MA). Images were obtained on the Zeiss Axiovert microscope using the 655-nm custom filter set described in the previous chapter, and then converted to jpg using Axiovision software (ver 4.3, Carl Zeiss Vision, Germany).

A routine was developed for reconstructing the 3-D distribution of QD-hMSCs injected into rat hearts. Tissue was processed as described above and 222 (rat terminated at 1 hour) or 126 (rat terminated at 1 day) serial transverse 10-μm-thick sections were imaged for both QD (655-nm) fluorescence and phase contrast on the Axiovert deconvolution microscope with the 2.5X objective. Using Axiovision software, fluorescence and phase images for each section were merged to generate jpg images. The remaining image processing was executed in Matlab. Phase contrast features echoed in each serial section were identified and the coordinates were used to spatially register the images with respect to one another. These registered RGB jpgs were converted to HSV format and the saturation and value channels were used to create new intensity images bearing only the QD-positive regions. These were then thresholded to generate binary maps, where white pixels represent all of the QD-positive zones. All of the QD-positive cells that were not contained within the cardiac syncytium (cells remaining in the adhesive on the epicardial surface) were eliminated from the reconstructions. The binary maps for all of the serial sections were combined into a 3-D matrix, and the total area (or volume) of white pixels was computed. High-resolution images (63X) were obtained and areas of single cells were determined similar to the method described in the previous chapter. Thus, the number of cells in the reconstruction was calculated by dividing the total 3-D area by the average area of QDs per cell in a section. The centroid was determined for each individual polygon in the volume matrix, and then weighted to the

polygon volume to find the centroid of the total cell mass. Next, the distance was calculated between each individual cluster and the centroid of the cell mass to characterize the distribution of QD-hMSCs in the tissue. The distribution was visualized in 3-D by extracting isosurface data from the volume matrix and composing patch graphics objects for each of the continuous polygons in the matrix.

4.2.3 Results

Free QDs released into the extracellular space are not taken up by host cells

Although we performed several *in vitro* experiments to rule out potential false positives (see section 4.1.3), it was necessary to confirm these findings with an *in vivo* control. QDs can enter the extracellular space after *in vivo* delivery only if QD-labeled hMSCs die and leak their contents. We therefore performed the following experiment. The cell lysis product (mechanical lysis via shear stress through a 30-gauge needle) from approximately $1.5x10^5$ QD-hMSCs was injected into the left ventricular free wall of the rat heart. The injection site was demarcated with a small epicardial prolene suture. This experiment was performed in four animals, which were terminated at 1 hour (N=2) or 1 week (N=2) after the injection. Hearts were harvested, processed for sectioning and tissue sections were imaged for QD fluorescence. We did not observe QDs in any cell type in these hearts. This finding is expected, as free carboxylated QDs will be removed by the reticuloendothelial system in less than one hour[56].

The number and distribution of QD-hMSCs injected into the rat heart can be reconstructed in 3-D

Our laboratory has previously injected 1 million hMSCs transfected with the pacemaker gene HCN2 into the canine heart and used traditional immunocytochemistry to identify some of these cells in histologic sections[3]. We were unable, however, to enumerate all of the delivered cells in the host tissue and characterize their complete distribution. It was with that goal in mind that we injected approximately 100,000 QD-hMSCs into the left ventricular free wall of adult rat hearts. Specimens were harvested at either 1 hour (N=1), 1 day (N=1), 2 days (N=1) or 1 week (N=1) after injection and processed for sectioning on a cryostat. Serial 10-μm transverse sections were imaged for QD fluorescence (Figure 4.2.1a). Using algorithms described in Methods, these fluorescence images were filtered and thresholded to generate binary maps of QD-positive zones from all of the tissue sections (Figure 4.2.1b). The spatial locations of QD-hMSCs were identified from the series of binary maps and visualized in 3-D for the animals terminated at 1-hour (Figure 4.2.1c) and 1-day (Figure 4.2.1d) after injection. In these two experiments, we were able to enumerate the total number of QD-hMSCs in the whole hearts from the 3-D models (approximately 50,000 at 1 hour and 30,000 at 1 day). We also computed a distance parameter to characterize the distribution of cells, based on the distance between individual cells and the centroid of the total stem cell mass. Most of the cells at both time points were clustered in close proximity (>80% of cells within 1.5mm, see Figure 4.2.1f). However, there was a distinct difference in the spatial orientation of the stem cells between the 1-hour and 1-day hearts. At 1 hour, QD-hMSCs were not organized relative to myocyte orientation (Figure 4.2.1a), while at 1 day there

was clear evidence of stem cell alignment along the longitudinal axis of the myocyte bundles (Figure 4.2.1e). Twenty-four hours is roughly the time period necessary for significant gap junction formation[53].

The QD-hMSCs in tissue sections from the rat terminated 2 days after injection were more sparse compared to the earlier time points. At 1 week after injection, no QD-hMSCs were observed in tissues sections from these hearts.

QD-hMSCs can be transfected to overexpress a key pacemaker gene

Our laboratory has studied biological pacemakers that consist of hMSCs transfected to overexpress the HCN2 gene. This gene expresses a time dependent inward current, which is the basis of cardiac pacemaker activity. Since transfected hMSCs are our platform for gene delivery to the heart, if QDs are to be used as a tracking tool, they must not alter expression of the transgene. We performed an *in vitro* experiment to determine whether the presence of intracellular QDs would affect expression of exogenous genes. We transfected QD-hMSCs and unloaded hMSCs with the HCN2-pIRES-EGFP plasmid. After 48-hours, both unloaded and QD-loaded hMSCs were visualized for GFP expression and their expression levels were qualitatively compared. Similar levels of expression were apparent in both groups. GFP-positive cells from each group were then selected for patch clamping to record membrane currents (Figure 4.2.2). QD-hMSCs expressed the HCN2 gene and generated a family of pacemaker currents similar to those recorded in unloaded cells. The current amplitudes recorded at -150mV for both control and QD-hMSCs were -1459.48 ± 616.83 and -1352.68 ± 864.70 respectively ($p>0.05$, $N=5$ per group). From these experiments, we concluded that QDs do not interfere with exogenous gene transfection or expression and that QD-hMSCs can be used for functional pacemaker experiments in animal models.

4.2.4 Discussion

The experiments described above demonstrate that QDs can be used as a robust method of identifying pre-labeled exogenous cells in histologic tissue sections. This method obviates the need for any post-hoc immunostaining because of the QDs' inherent brightness. This feature allowed us to easily and quickly obtain hundreds of low-power images of QD-positive cells amidst native tissue. The rate limiting factor in this process is merely the time it takes to section the tissue. As an additional control, we demonstrated that free QDs from potentially dying QD-hMSCs are not taken up by host cells resident in the heart *in vivo*.

With stacks of images of these sections containing all of the QD-positive cells we were able to generate 3-D reconstructions of the QD-hMSCs *in vivo* in a manner akin to the way computed tomography works. From these 3-D models we enumerated the cells at the different time points and visualized changes in spatial geometry. At 1 hour after injection, the delivered hMSCs were diffusely located around the injection site, and did not appear organized with respect to the host tissue. Conversely, after 24 hours *in vivo*, the delivered cells were more tightly clustered in a given 10-μm section and tended to align along the host tissue myofibrils. The time period of these changes is consistent with hMSC-hMSC and hMSC-myocyte gap junction formation. Therefore, stem cells may be communicating with the native myocardium and organizing into some preferential

configuration. It is important to note that at neither time point did stem cells wander significantly from the site of injection.

When tissue from rats terminated at time points beyond 1 day was examined, a clear trend was observed. In the 2-day-post-injection rat, QD-hMSCs were decreased in number and much less tightly clustered than at earlier time points; at 1-week, no QD-hMSCs were identified in the entire heart. The timing of these findings is consistent with immune rejection of the human cells by the rats; xenografts are rejected within 2 to 3 days after transplantation by both direct and indirect pathways involving T-cell recognition of xenoantigens[57]. Although other experiments from our laboratory have demonstrated that hMSCs are immunopriviliged in the canine, there is no data to suggest that they are immunologically tolerated by rats. It has been suggested that MSCs prevent T-cell maturation and proliferation via either direct cell-to-cell effects or by secreting soluble factors[21]. But MSCs also express an array of surface adhesion molecules that function as ligands for inflammatory cells; it is therefore reasonable to expect that under certain conditions and in some animal models, xenographic MSCs (i.e. hMSC delivery to a rat) may evoke an immune response.

Because one long-term goal of the work in our lab is the use of hMSCs for the creation of biological pacemakers *in vivo*, we tested whether the presence of QDs in these cells would affect gene expression after transfection. We found that after transfection with a key pacemaker gene (HCN2), QD-hMSCs expressed a family of pacemaker currents similar to those expressed by unlabeled hMSCs. It should therefore be feasible to use QDs to track HCN2-hMSCs in future biological pacemaker studies.

In summary, by using QDs for stem cell location tracking, we were able to generate the first complete single-cell resolution quantitative representations of the distribution of delivered stem cells *in vivo*.

Figure 4.2.1. QDs can be used to identify single hMSCs after injection into the rat heart and further used to reconstruct the 3-D distribution of all delivered cells
Rat hearts were injected with QD-hMSCs. Fixed, frozen sections were cut transversely (b, inset) at 10-μm and mounted onto glass slides. Sections were imaged for QD fluorescence emission (655nm) with phase overlay to visualize tissue borders. QD-hMSCs can be visualized at (a) low power, and (a, inset) high power (Hoechst 33342 dye used to stain nuclei blue). In (a, inset), endogenous nuclei can be seen adjacent to the delivered cells in the mid-myocardium (arrows). Serial low power images were registered with respect to one another and (b) binary masks were generated, where white pixels depict the QD-positive zones in the images. The vertical line in (b, inset) represents the z axis, which has a zero value at the apex of the heart. The binary masks for all of the QD-positive sections of the heart were compiled and used to generate the 3-D reconstruction of delivered cells in the tissue. QD-hMSCs remaining in the tissue adhesive on the epicardial surface (and not within the cardiac syncytium) were excluded from the reconstruction. (c) QD-hMSC reconstruction in an animal that was terminated 1 hour after injection. (d) Reconstruction from an animal euthanized 1 day after injection with orientation noted in inset. Our reconstructions in (c) and (d) do not account for all of the approximately 100,000 hMSCs delivered through the needle. Some of these cells undoubtedly leaked out of the needle track, while others may not have survived the injection protocol. The views of both reconstructions (c) and (d) are oriented for optimal static visualization (and also have different scales and are situated at different positions along the z-axis depending on the distance of the injection site from the apex of the heart). (e) One day after injection into the heart, the pattern of QD-hMSCs is well organized and appears to mimic the endogenous myocardial orientation (dotted white line highlights myofibril alignment). Complete representations of the spatial localization of QD-hMSCs in the heart permits further quantitative analyses. (f) One parameter that can be computed is the distance of individual cells from the centroid of the total stem cell mass. The plots show the percentage of stem cells at a distance less than or equal to x for both the 1-hour and 1-day rats. At both time points, most of the cells are within 1.5mm of the centroid.
Scale bar on a = 500μm, inset = 20μm
Scale bar on b, inset = 1 cm
Scale bar on e = 500μm

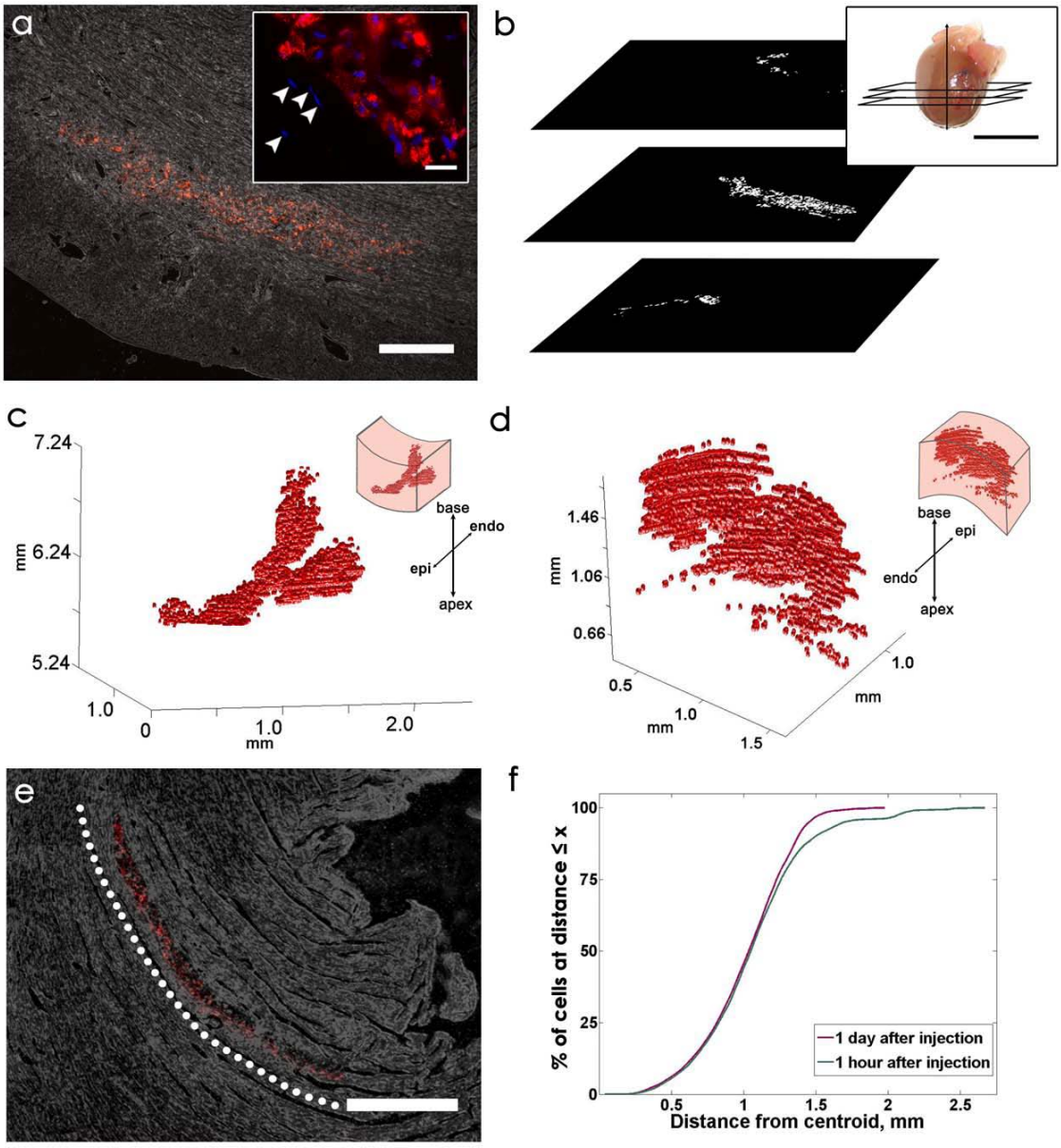
a
b
c
d
e
f
7.24
6.24
5.24
mm
1.0
0
1.0
2.0
mm
base
endo
epi
apex
1.46
1.06
0.66
mm
0.5
1.0
1.5
mm
1.0
base
epi
endo
apex
100
75
50
25
0
% of cells at distance ≤ x
0.5
1
1.5
2
2.5
Distance from centroid, mm
1 day after injection
1 hour after injection

Figure 4.2.2. The presence of intracellular QDs does not affect ability of cells to overexpress genes after transfection

QD-hMSCs and plain hMSCs were each transfected with the HCN2-pIRES-EGFP plasmid via electroporation. Two days after transfection, both groups of cells expressed similar levels of GFP (data not shown) and cells expressing GFP from both groups were patch clamped to record the HCN2-induced currents. The currents provided were from a holding potential of -40mV and included steps to between -40mV and -160mV in -10mV increments. Similar levels of HCN2-induced current were recorded from (a) unloaded and (b) QD-loaded hMSCs. Additionally, the electroporation process did not alter the cytoplasmic distribution of QDs (b, inset). Imaging for these experiments was carried out on the Olympus microscope using the Texas Red filter to visualize QDs in live cells; this filter set does not optimally visualize QD loading. Jia Lu performed the path clamp recordings.

Scale bar on b inset = 50μm

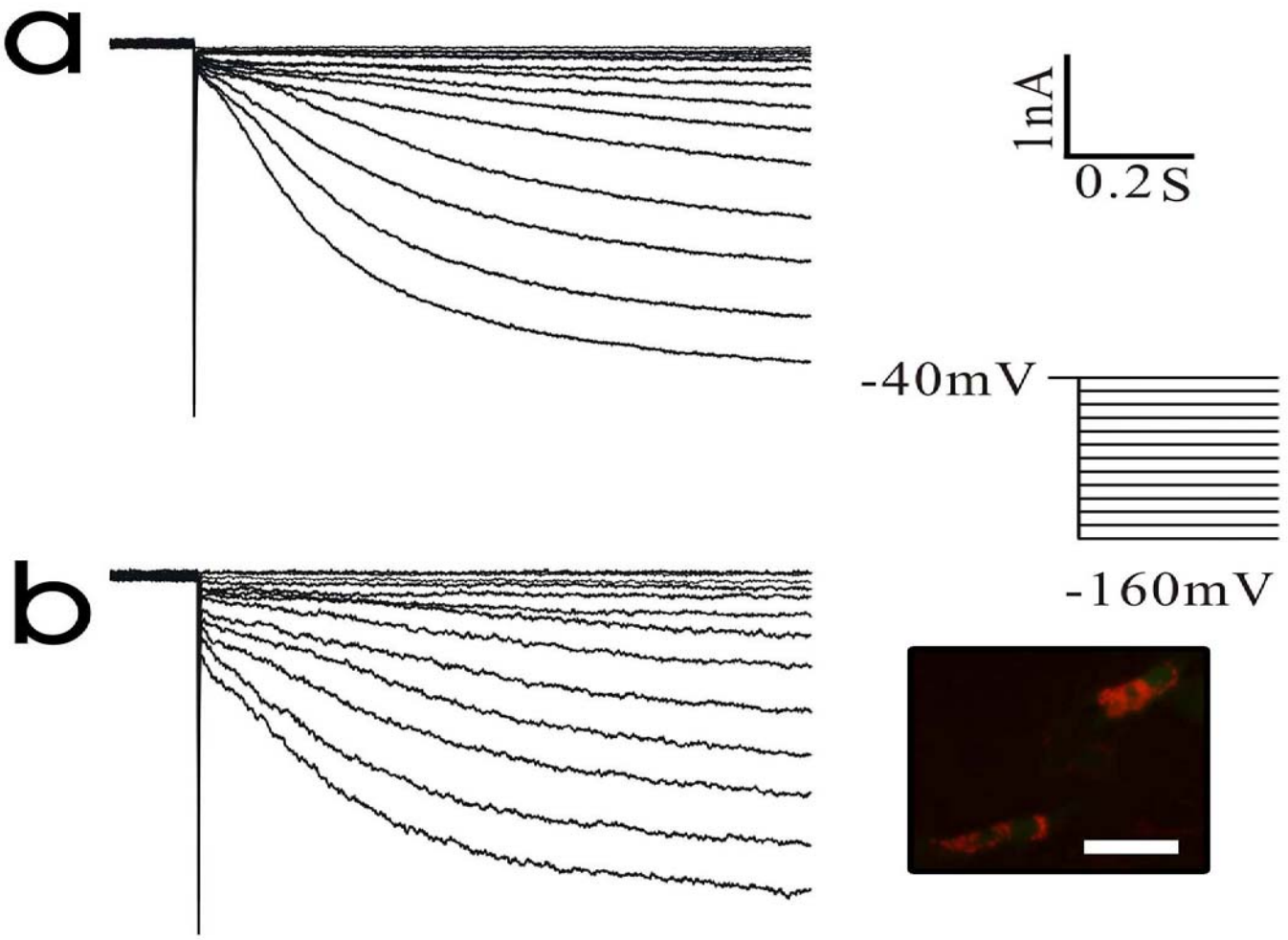
a
1nA
0.2S
-40mV
b
-160mV

4.3 The fate of QD-cardiogenic hMSCs can be tracked after in vivo *delivery for up to 8 weeks*

4.3.1 Introduction

hMSCs are a dynamic cell type, capable of either remaining undifferentiated or differentiating along mesodermal lineages. While we can exploit the former property for our biological pacemaker experiments (see section 4.2), we are also interested in using hMSCs to repair functional contractile myocardium. For this application, hMSCs must be induced to differentiate along a myocyte lineage. Our laboratory has developed an *in vitro* method to partially commit hMSCs toward a cardiomyocyte fate (cardiogenic cells)[6]. We have delivered hMSCs or cardiogenic cells to the canine heart via an extracellular matrix scaffold and measured improved functional recovery in the region of the patch 8 weeks after delivery with cardiogenic cells vs. hMSCs[6]. These experiments suggest that cardiogenic cells might terminally differentiate into mature myocytes that contribute to regional work.

In order to correlate any measured functional recovery with structural evidence of myocyte formation, we must pre-label the cells, identify them in histologic sections and then use immunostaining methods to see if they express cardiac-specific markers. In this chaper, we will demonstrate that both hMSCs and cardiogenic cells can be labeled with QDs prior to delivery. We have identified QD-positive cells in histologic sections from regions of extracellular matrix patch implants, and shown that hMSCs and cardiogenic cells differentiate into endothelial and myocyte fates respectively. Successful fate tracking relies first on the ability to identify the delivered cells in hisologic sections. Cell tracking with traditional agents like GFP has previously failed in this regard because of the extremely high levels of autofluorescence in the damaged myocardium[27]. But by using QDs, we can now identify delivered cells after prolonged periods *in vivo* and characterize their fate.

4.3.2 Methods

In vivo studies

All animals received humane care in compliance with the *Principles of Labroatory Animal Care* formulated by the National Society for Medical Research and the *Guide for the Care and Use of Laboratory Animals* prepared by the National Academy of Sciences and published by the National Institutes of Health (NIH Publication No. 85-23, revised 1985). The animal protocols used were approved by the IACUC at Stony Brook University.

Gene transfections

For some experiments, hMSCs were transfected with the Wnt5A (4 μg, pUSEamp, Upstate Cell Signaling Solutions, Figure 4) or pIRES-EGFP (4 μg) plasmid using the Amaxa biosystems nucleofection technique[3].

Formation of cardiogenic cells

hMSCs were loaded with QDs as described in the previous chapter and formed into embryoid bodies[6]. Briefly, roughly 125,000-250,000 cells were suspended in 10-μl DMEM-10%FBS and suspension droplet was placed onto the cover of a tissue culture dish, which was then inverted. Cells in the hanging droplets began to aggregate over several hours, and media was replaced daily for 3 days.

Preparation of ECM patches

A 15x30x0.1mm acellular extracellular matrix (ECM) patch (AcellVet) was rinsed twice in PBS for 10 minutes each. The patch was then soaked in MSCGM for 15 minutes, after which time the media was removed. QD-GFP-hMSCs, QD-Wnt5A-hMSCs or QD-cardiogenic cell embryoid bodies were then seeded directly onto the ECM. The patch was returned to 37^{o}C for approximately 12 hours prior to implant.

Surgical procedures

A thoracotomy was used to expose the heart. A vascular clamp was then used to isolate a region of the right ventricular free wall. A full thickness defect was surgically induced and the cell-seeded scaffold was used to replace it. The chest was closed and the animal was allowed to recover. Animals were sustained under veterinary care and humanely terminated by an approved protocol at 8 weeks with pentobarbital.

Immunohistochemistry

Tissue samples from the implant region and control myocardium were explanted, fixed in 4% paraformaldehyde for 24 hours, and then transferred to 30% sucrose solution. Tissue blocks were embedded for frozen sectioning at 10-μm. Sections or CC2-coated chamber slides containing cells (hUVECs or hMSCs) were hydrated with PBS, permeablized with 0.5% Tween-20 in 1X TBS followed by 0.25 % Triton X-100 in TBS, and then blocked with normal horse serum (Vector, Burlingame, CA). Staining for CD31 was performed as follows: samples were incubated for 4 hours in FITC-conjugated anti-human CD31 (Diaclone, Stamford, CT). Control samples were incubated in PBS instead of the antibody. Samples were washed in PBS, incubated with 1μM Hoescht33342 for 20 minutes (Invitrogen, Carlsbad, CA), then washed in PBS before mounting with Vectashield (Vector, Burlingame, CA). Staining for sarcomeric α-actinin was performed as follows: sections were incubated in primary antibody directed against sarcomeric α-actinin (Sigma-Aldrich, St. Louis, MO). Sections were then incubated with a biotinylated secondary antibody (Vector Laboratories, Burlingame, CA) and finally, incubated with streptavidin-conjugated near infrared-emitting quantum dots (705nm, Invitrogen Corp., Eugene, Oregon).

Fluorescent images were acquired with a Zeiss Axiovert 200M fluorescent microscope in z-stack mode and were deconvolved with the AxioVision software package (Carl Zeiss) to obtain confocal quality optical sections. Some image stacks were post-processed in ImageJ (NIH, Bethesda, MD). Custom filters were used to image quantum dot fluorescence (Omega Optical, Brattleboro, VT).

4.3.3 Results

QD-hMSCs can be visualized to the exclusion of autofluorescence

hMSCs were dual labeled by both loading with QDs and transfecting the cells to express GFP. The cells were seeded onto a 100-μm-thick extracellular matrix (ECM) patch and incubated for 24 hours at 37^{o}. The patch was fixed and mounted under a glass coverslip with the cell-side facing up as described in Chapter 4.1. The slide was inverted onto the transillumination microscope and imaging for cellular fluorescence was performed through the full thickness of the patch (Figure 4.3.1b). Regions of the patch were imaged for GFP fluorescence, but cell features were not apparent and only autofluorescent variations in the matrix were visualized (Figure 4.3.1c). When the same regions were imaged for QD fluorescence using custom QD filters that excite at a wavelength much less than the wavelength of emission the intracellular QDs were clearly visible (Figure 4.3.1d). Autofluorescence is not collected when imaging with the QD filters. The exposure times of incident fluorescence used to image for GFP (Figure 4.3.1c) and QD (Figure 4.3.1d) were 22 and 190 ms respectively.

QD-hMSCs can be identified in canine myocardium 8 weeks after delivery

QD-Wnt5a-hMSC-seeded scaffolds (15x30x0.1mm, porcine urinary bladder ECM, AcellVet) were used to replace surgically-induced full thickness myocardial defects. Tissue was excised and processed for analysis. Histologic sections were imaged for QD fluorescence and QD-hMSCs were identified (Figure 4.3.2b). The pattern of QD fluorescence was still diffuse (Figure 4.3.2b, inset), but dilution of the label appeared to have occurred over the 8 weeks *in vivo*. Even still, the QD fluorescence intensity far surpassed that of host tissue autofluorescence and specific detection of the exogenous cells was still possible at 8 weeks.

QDs do not affect differentiation of hMSCs *in vivo*

hMSCs have been found to spontaneously differentiate along an endothelial lineage and participate in angiogenesis in response to tissue injury[58]. We sought to determine whether the presence of QDs in these cells would affect their ability to develop an endothelial fate. Histologic sections from an explanted 8-week old QD-Wnt5A-hMSC ECM patch were stained for the marker CD31 (PECAM-1) using a human-specific antibody. Many of the QD-containing regions in these sections stained positively for CD31 (Figure 4.3.3a), with several areas showing clear co-localization (Figure 4.3.3a inset), suggesting that these cells were differentiating along an endothelial lineage. As a means of control, endogenous canine endothelium from the same tissue sections were negative for the marker (Figure 4.3.3b), as were cultured hMSCs in vitro (Figure 4.3.3d), whereas human endothelial cells in culture stained positive (Figure 4.3.3c).

QD-cardiogenic cells differentiate into mature myocytes *in vivo*

As with the QD-hMSC patches, we identified QD-positive cells within the patch region of ventricle in which a QD-cardiogenic cell patch was implanted. Again, the

pattern of QD fluorescence was diffuse but appreciably diluted. Histologic sections in which QD-positive cells were identified were stained for the cardiac-specific marker, sarcomeric α-actinin. The region of tissue containing cardiogenic stem cells stained positively for this protein (Figure 4.3.4a). In addition, some of these cells appear to have differentiated into striated myocytes (Figure 4.3.4b,c) with appropriately-spaced (approximately 2μm) sarcomeres (Figure 4.3.4a, inset).

4.3.4 Discussion

In the previous chapter we discussed the use of QDs for tracking stem cell location *in vivo*. In this chapter, we demonstrate that one can extend this tracking for extended time periods and, once the labeled cells are identified, their fate can be determined.

Tissue engineering using biodegradable scaffolds has become a focus of regenerative medicine. Research in our lab has shown that such scaffolds are superior to traditional inorganic materials such as Dacron, for repair of a surgically induced myocardial defect[59]. We are interested in seeding these scaffolds with stem cells in order to enhance their reparative effects. One major limitation, however, has been that these relatively thick patch materials emit a significant amount of autofluorescence when excited by ultraviolet light. This prevents imaging of patches bearing cells labeled with traditional fluorescent markers (i.e. GFP). Imaging of these patches is important because of the need to enumerate the cells and determine cell confluency. We seeded an ECM patch with hMSCs that were co-labeled with both QDs and GFP. The patch was imaged for both QD and GFP fluorescence. GFP fluorescence from the cells on the patch was not discernable above autofluorescence, even though a very short exposure time was used to excite the tissue. In contrast, by using red QDs and custom filters, the intracellular QDs illuminated the cells on the patch to the exclusion of autofluorescence. These results reveal the benefits of using QDs for imaging in highly autofluorescent tissues, as explained in Chapter 2.

We induced a cardiac injury in canine ventricle via removal of a full thickness of myocardium, and replaced this site with an ECM patch onto which QD-hMSCs were seeded. After 8 weeks, QD fluorescence was clearly visible in the injured tissue well above high levels of autofluorescence. Therefore, we have shown that QDs successfully illuminate delivered hMSCs even in damaged myocardium.

By staining tissue in which QD-hMSCs were identified for a human-specific antibody against CD31, we showed that some of the stem cells were adopting an endothelial fate. From this result, together with the data presented in Chapter 4.1 (*in vitro* differentiation), we conclude that the presence of QDs within the cytoplasm does not affect the ability of hMSCs to differentiate. Furthermore, terminally differentiated cells retain the QD label. Together, this tells us that QDs can be used to track stem cell fate after delivery *in vivo*.

We have previously reported both cellular and functional cardiac regeneration after replacing a full thickness right ventricular defect in the canine heart with an acellular ECM patch derived from porcine urinary bladder[59]. Our laboratory has also developed a novel method of partially differentiating hMSCs along a cardiac lineage[6]. If a naked ECM patch induces regeneration, we thought it might be possible to enhance the regeneration process by delivering cardiogenic stem cells on a patch. We therefore

implanted ECM patches (~15x30x0.1 mm) seeded with QD-cardiogenic cells, terminated the animals 8 weeks after implantation and excised a region of myocardium circumscribing the patch implant area for analysis. Not only could we identify the QD-positive cells without any detectable contribution from background autofluorescence, we also showed that these cells express the cardiac-specific protein sarcomeric α-actinin. The expression of this protein was somewhat disorganized in the center of the patch implant area. But, at the border with the native myocardium, QD-cardiogenic cells expressed sarcomeric α-actinin in a banding pattern that resembled sarcomere formation. Upon further inspection, we observed that the distance between these bands was consistent with that of myocytes in the native tissue, suggesting that some QD-cardiogenic cells were becoming mature myocytes.

Ongoing work in our laboratory has in fact shown that, based on a high density mapping (HDM) method for measuring surface deformation of myocardium[60], functional recovery is improved when ECM patches used to replace full thickness defects are seeded with cardiogenic stem cells. Could this be due to transdifferentiation of these cells into mature myocytes? By using QDs to track stem cells *in vivo*, questions of long term fate can now be addressed.

When staining for sarcomeric α-actinin we used a quantum dot-conjugated secondary antibody. This allowed us to capitalize on the many advantages of QDs over traditional staining fluorophores. Using a QD-antibody allowed us to have more confidence in the staining outcome, because of the lack of contribution from autofluorescence. This also represents an example of multiplexing, because we were able to image two different color QDs in the same field with no spectral overlap.

Figure 4.3.1. QDs illuminate hMSCs above autofluorescence through an ECM patch while GFP does not

hMSCs were co-labeled by loading with 655-nm QDs and transfection with green fluorescent protein (GFP) and then seeded onto a 100-μm-thick extracellular matrix patch. (a) The patch was mounted under a coverslip with the cells facing up and (b) inverted onto the inverted microscope such that the exciting UV light passes through the full thickness of the patch. (c) The patch is imaged using the GFP filter, but cells are not discernable above the autofluorescence of the matrix. (d) When the same region is imaged using custom QD filters, fluorescence emitted from the QDs is detected without any contribution from autofluorescence.

Scale bar on c,d = 25 μm

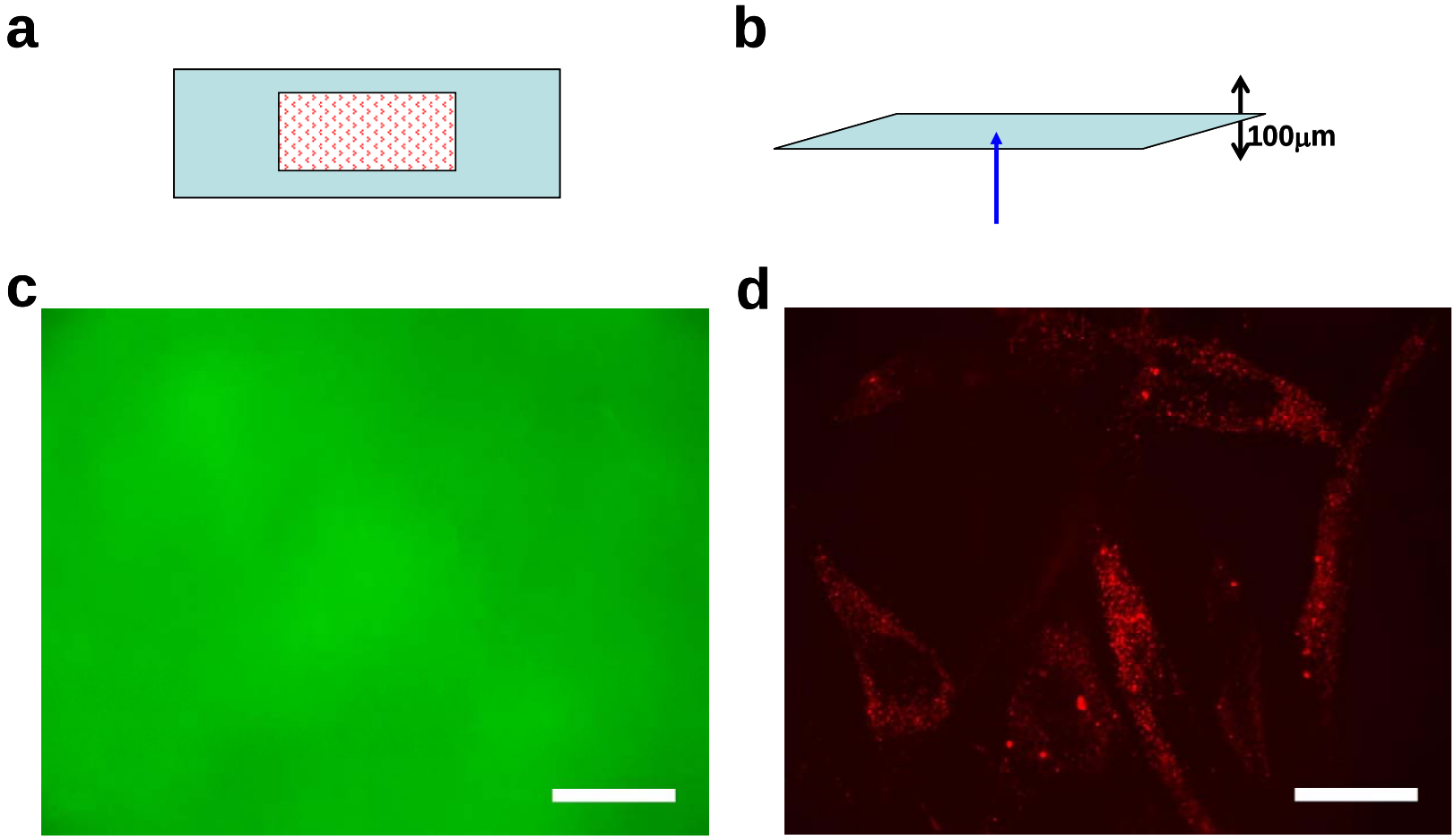
a
b
100µm
c
d

Figure 4.3.2. QD-hMSCs can be delivered to the canine heart on an ECM scaffold and identified 8 weeks later

QD-hMSCs were delivered to the canine ventricle via implantation of an ECM patch. Eight weeks later, tissue was explanted and fixed. Panel (a) shows fixed tissue from one animal with a blue line circumscribing the region analyzed (and imaged transmurally in panel c) and a black dotted ellipse approximating the patch borders. Straight dark black lines in the image are dissecting pins that were used to secure the tissue while photographing. The region outlined in blue was (a) frozen and sectioned transmurally at 10-μm and (b) imaged for QD fluorescence (655nm) and phase contrast. (c) The plane of section is transmural from epicardium (top) to endocardium (bottom); a green circle highlights the region where QDs were found (imaged in b). Some tissue sections were stained with Hoechst 33342 to visualize nuclei. Panel (b, inset) shows QD-hMSCs amidst endogenous tissue (asterisks denote endogenous nuclei).

Scale bar on a, c = 20 mm

Scale bar on b = 50 μm, inset = 10 μm

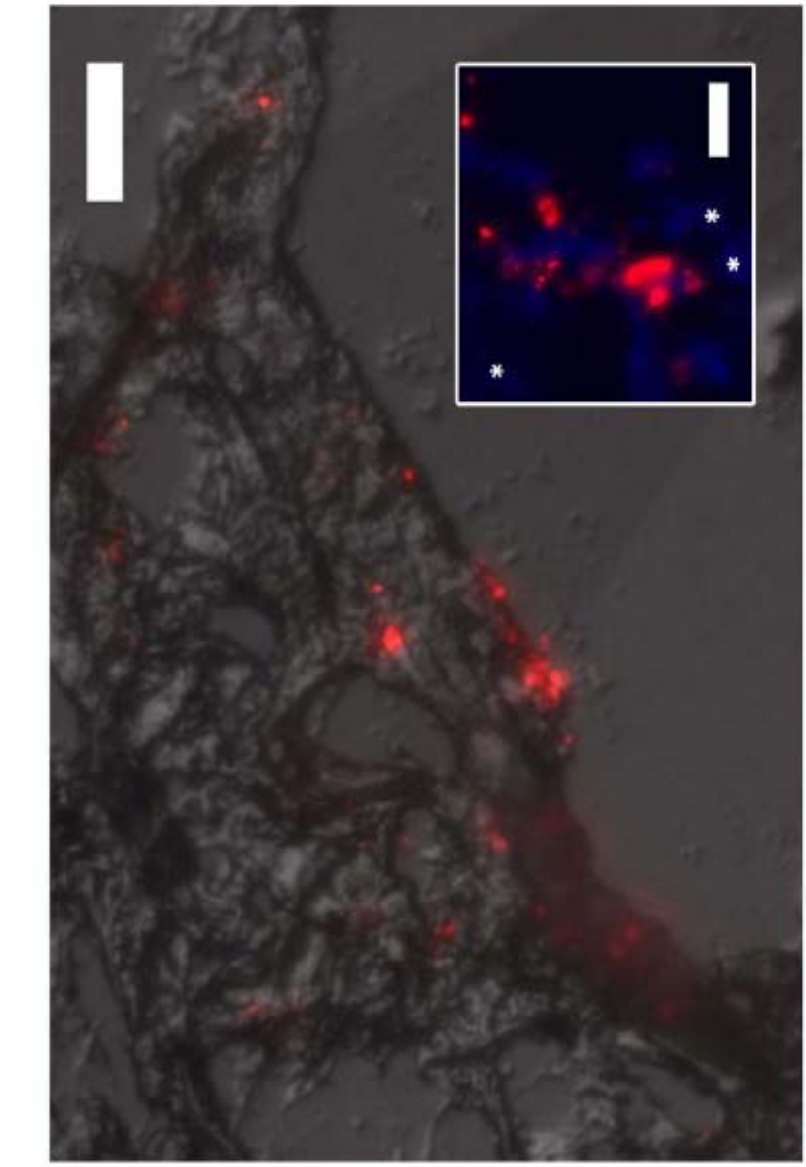

b

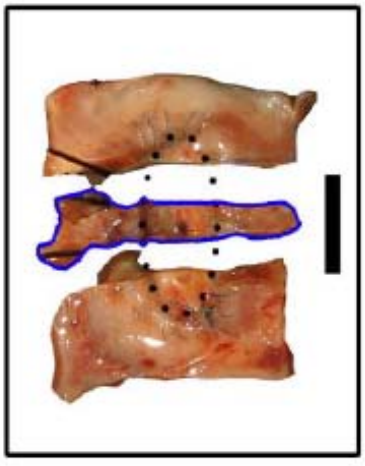

a

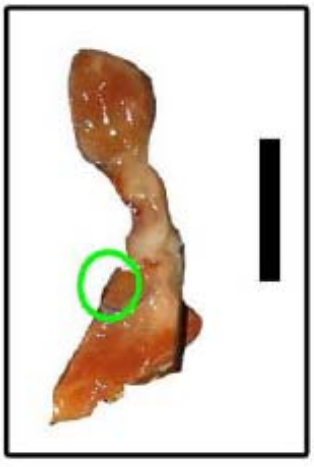

c

Figure 4.3.3. QDs do not interfere with differentiation of hMSCs *in vivo*
(a) After 8 weeks, some of these QD-positive cells (red) express the endothelial marker PECAM-1 (green), suggesting differentiation of these cells along an endothelial lineage. A high-power view of QD-positive cells with co-localized PECAM-1 expression is shown in (a, inset). In these images, exposure times for obtaining QD fluorescence were selected to avoid overexposure in the regions of higher QD density, and may therefore fail to visualize all QD-positive cells. Controls include: (b) host canine endothelial cells seen lining the lumen of a blood vessel do not stain positively for the anti-human CD31, emphasizing the species-specificity of the antibody (same microscope and camera settings for imaging as in a); (c) Cultured human endothelial cells express but (d) cultured hMSCs do not express the anti-human CD31. (e) Negative control human endothelial cells without exposure to the FITC-conjugated anti-CD31 antibody. Insets in (c),(d), and (e) show higher power views (630X) of individual cells. Images in (c),(d), and (e) and respective insets acquired using same microscope and camera settings per objective.
Scale bar on a = 20 μm, inset = 5 μm
Scale bar on b = 20 μm
Scale bar on c,d,e = 50 μm, insets on c,d,e = 20 μm

a
b
c
d
e

Figure 4.3.4. QD-cardiogenic cells express cardiac proteins and demonstrate features of functional myocytes after 8 weeks in vivo.
Tissue sections in which QD-cardiogenic cells were identified were stained for the cardiac-specific protein α-sarcomeric actinin. (a) QD-cardiogenic cells expressed α -sarcomeric actinin, with staining intensity comparable to that seen in regions of neighboring myocardium. (b) QD-cardiogenic cells were apparent at the patch border where sarcomere structure transitioned from organized (neighboring myocardium, inset) to disorganized. (c) Some QD-cardiogenic cells demonstrated regular sarcomere spacing (approximately 2μm), suggesting that these cells had terminally differentiated into functional myocytes.

a

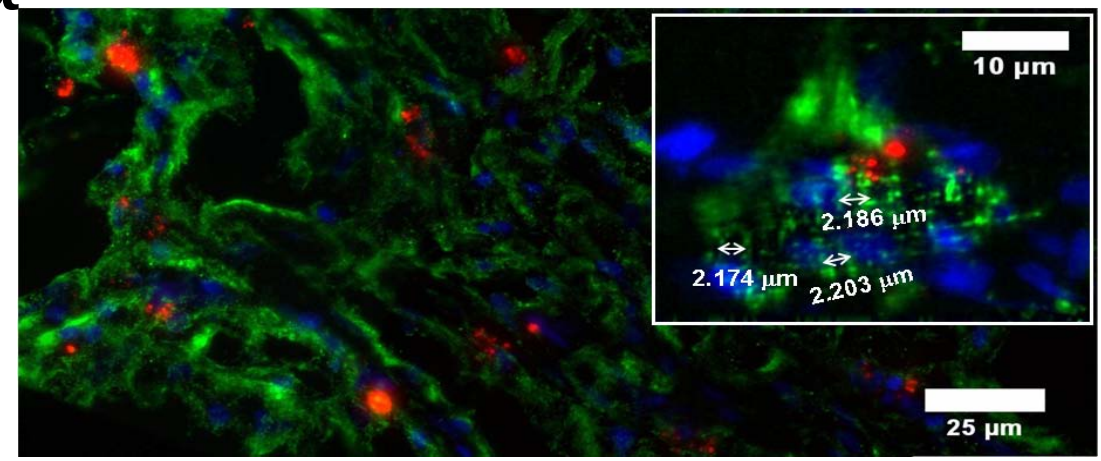

b

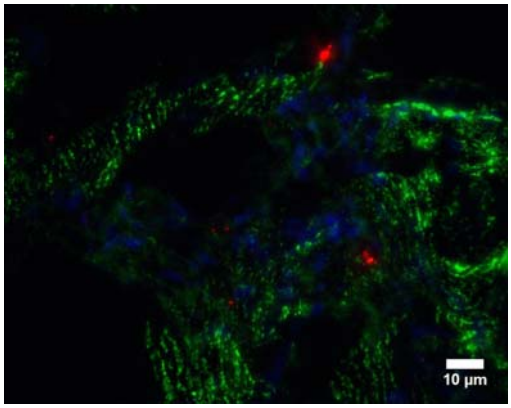

c

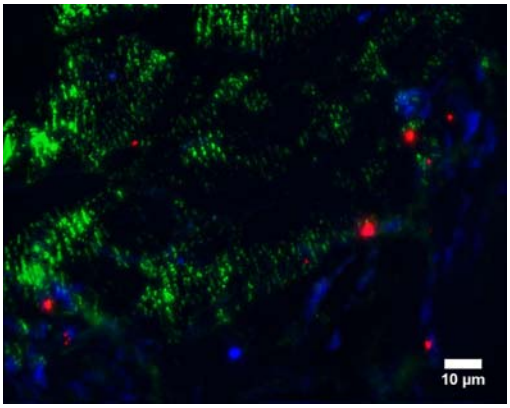

d

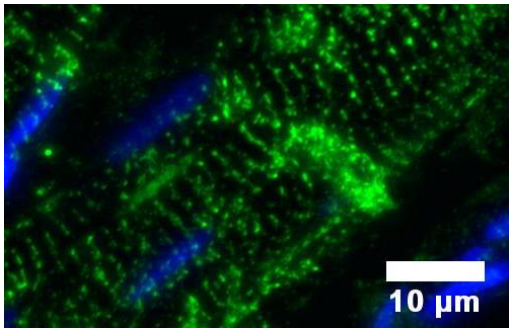

4.4 QDs can be used to track labeled hMSCs non-invasively in vivo

4.4.1 Introduction

The previous two chapters described a method that necessitates termination of the animals in order to excise tissue samples and image histologic sections. However, the long term future of stem cell therapies will depend on the ability to track non-invasively.

Both the core of the QD and the passivating shell contain metal ions (cadmium and zinc respectively). Metals are radiopaque, meaning they do not allow penetration of x-ray waves, and can therefore be imaged using x-ray technology. Traditional x-rays are too large to interfere with nano- or micro-scaled metals. However, since they are radiopaque, it might be possible to use micro computed tomography (μCT) scanning to image QDs *in vivo*.

4.4.2 Methods

Preparation of cells for phantom

QD-hMSCs were prepared as described in Chapter 4.1.2. After 24 hours, cells were washed and visualized to confirm QD loading (Figure 4.4.1a). Cells from the QD-hMSC group and a separate control unloaded hMSC group were each trypisinized and centrifuged at 1000g for 4 minutes in polypropylene tubes to prevent adhesion of cells to tube walls. The pellets were resuspended in MSCGM and the solution was then centrifuged at 1500g for 5 minutes. Pellets were incubated at 37^{o}C overnight. After the incubation period and without breaking them up, pellets were gently washed in PBS and fixed in 4% paraformaldehyde for 2 hours.

Creation of phantom mold

A curable siloxane compound was prepared by mixing vinylmethylpolysiloxane (GE silicones RTV615A, s.d.1.02 g/cm^3) and vinyl MQ resin (GE silicones RTV615B, s.d.0.99 g/cm^3) in a 10:1 ratio and stirring for 5 minutes. The mixture was then poured into two wells of a 4-well chamber slide to cover the bottom of the well and cured at 50^{o}C for 2 hours. The cell pellets were placed in each well and additional siloxane mixture was poured over the top to complete cover the pellets. The materials cured overnight at room temperature (Figure 4.4.1b).

μCT scanning

High resolution (9μm) μCT scanning (Scano Medical μCT 40, Basserdorf, Switzerland) was used to visualize cell pellets within the siloxane mold. Individual 2D images from the unloaded hMSC and QD-hMSC molds were visualized and densities in the cell pellet regions were measured from image intensities (12 and 16 images sampled respectively). A constrained 3D Gaussian filter was applied to reduce noise in the images ("support"= 9, "sigma"= 5). Cell pellet regions were segmented from the surrounding siloxane by thresholding (lower threshold = 124, upper threshold = 1000). The 3D reconstruction was generated from the stack of binarized images.

Statistics

All data are listed as mean ± standard deviation. Data sets were compared by a Student's t-test with $p<0.05$ considered significant.

4.4.3 Results

Theoretical feasibility

QDs are semiconductor nanoparticles comprised of a CdSe core and ZnS shell. Because of the very high densities of these materials (5.816g/cm^3 and 4.09g/cm^3 respectively), we investigated whether QD-hMSCs could be imaged using micro-computed tomography (μCT) scanning. In order for QD-hMSCs to be detected within a block of tissue, two criteria must be satisfied: 1) the resolution of the CT scanner must be sensitive enough to detect single cells (mean diameter, 10μm) and 2) the overall physical density of a QD-loaded hMSC must be at least 10% higher than the physical density of the surrounding tissue. Currently, micro CT (μCT) scanners are available with resolutions as low as 1μm. At Stony Brook there is a μCT scanner with 6μm resolution so this should satisfy the first criterion listed above.

After uptake by hMSCs, QDs exist within the cells in clusters with an average diameter of 0.75μm (see chapter 4.1). Prior to cell division the average cell contains approximately 200 of these QD clusters, as determined by fluorescence imaging. Since an individual cluster will occupy approximately 0.22μm^3 in the cell, the total volume of QDs in a given cell is roughly 44μm^3. An average hMSC has a volume of approximately 500μm^3. Therefore, based on these calculations, QDs occupy approximately 9% of the volume of the cell. This is a low-end estimate of the percent volume, with alternate calculations yielding a value as high as 25%. Assuming a cell and tissue density of 1.05g/cm^3, the expected overall physical density of QD-hMSCs should range from 1.14-2.00g/cm^3. These densities are well above the threshold for detection of the μCT scanner currently available at Stony Brook.

Based on these findings, it is theoretically feasible for QD-hMSCs to be detected with μCT in both explanted tissue samples and in living animals.

μCT testing

Both unloaded hMSC and QD-hMSC pellets were detectable within the siloxane mold (Figure 4.4.1c) as areas of hypointensity. Regions of interest within the pellet area from sample images in each group were selected in order to measure densities (N=12 for unloaded hMSC, N=16 for QD-hMSC). Density measurements were normalized to the average density of the unloaded hMSC pellet. The values were 1.000 ± 0.103 and 1.276 ± 0.039 for unloaded and QD-hMSC pellets respectively (Figure 4.4.1d). A 3-D reconstruction of the QD-hMSC pellet was generated from the stack of images (Figure 4.4.1e).

4.4.4 Discussion

What might be considered the "holy grail" of stem cell tracking is the development of a tracking agent that can visualize delivered cells *in vivo* non-invasively

with high resolution. Existing techniques for non-invasive tracking of stem cells include loading cells with radioactive substances like truncated thymidine kinase for positron emission tomography (PET) detection[61, 62] or radiometals for single photon emission computed tomography (SPECT)[35]. Concerns have arisen, however, over the uptake of the label by host tissue, endogenous tissue photon attenuation and high levels of label needed for detection[9]. Another approach is the transfection of cells with the gene for luciferase; this allows cells to be visualized using bioluminescence. Major problems with this approach include the absorption and scatter of visible light and use of non-human genetic material[9]. More commonly used for non-invasive cell tracking are radioopaque metals like iron (super paramagnetic iron oxide, SPIOs)[30, 63] and gadolinium[64]. These materials are visualized using magnetic resonance imaging (MRI). For gadolinium, difficulties arise in loading the cells with sufficient concentrations to permit T1 contrast. Since high concentrations are needed, the dilution effects are pronounced as cells divide[9]. SPIOs like ferridex are most frequently used, but conflicting studies exist on whether these particles interfere with chondrogenesis[65-67]. If true, this would suggest they are not a "stealth" particle within the cell and could potentially interfere with other important physiologic functions. Further, should the technique be extended to clinical trials in humans, individuals with electronic pacemakers or implantable defibrillators would be excluded from the study[68]. This would isolate a potentially needy patient population.

In this chapter, we have shown that passive QD loading of hMSCs yields cells that are labeled with sufficient QD clusters to theoretically permit detection via μCT. When pelleted and embedded in a siloxane mold, the labeled cells are detectable and found to be approximately 27% denser than unlabeled cells. This result is consistent with theoretical calculations. Based on these findings, it should be possible to detect a cluster of QD-hMSCs within heart tissue using μCT.

Still, further experiments will be necessary before this approach can be applied in large animals. QD-hMSCs must be injected into heart tissue and the sample must be scanned to confirm feasibility. Then, non-invasive scanning can be tested in living animals. One potential hurdle that might be faced is the need to develop gating algorithms to synchronize the scanning with the heart beat. Scano Medical manufactures *in vivo* scanners for animals (vivaCT 40) and humans (XtremeCT) that have resolutions of 16 and 100μm respectively. These resolutions are acceptable (approximately single cell resolution for the animal scanner and 125-cell resolution for the human scanner) and superior to that attainable with SPIOs and MRI.

Figure 4.4.1. QDs can be visualized using μCT
QD-hMSCs were (a) loaded and imaged, and then formed into a pellet overnight. (b) The QD-hMSC pellet and a pellet formed from unloaded hMSCs were each embedded in a separate siloxane mold. Both phantom molds were scanned using μCT and images were reconstructed. In (c) a 2-D image of one section through the QD-hMSC pellet is shown. (d) Average densities for pellets formed from QD-loaded (N=16) and unloaded (N=12) hMSCs were calculated and normalized to the average density of the unloaded pellet. QD-hMSCs were roughly 27% denser than unloaded hMSCs. (e) The 3-D reconstruction of the scanned region of QD-hMSC pellet is shown.
Scale bar on a = 200μm
Scale bar on b = 1cm
Scale bar on c = 1mm

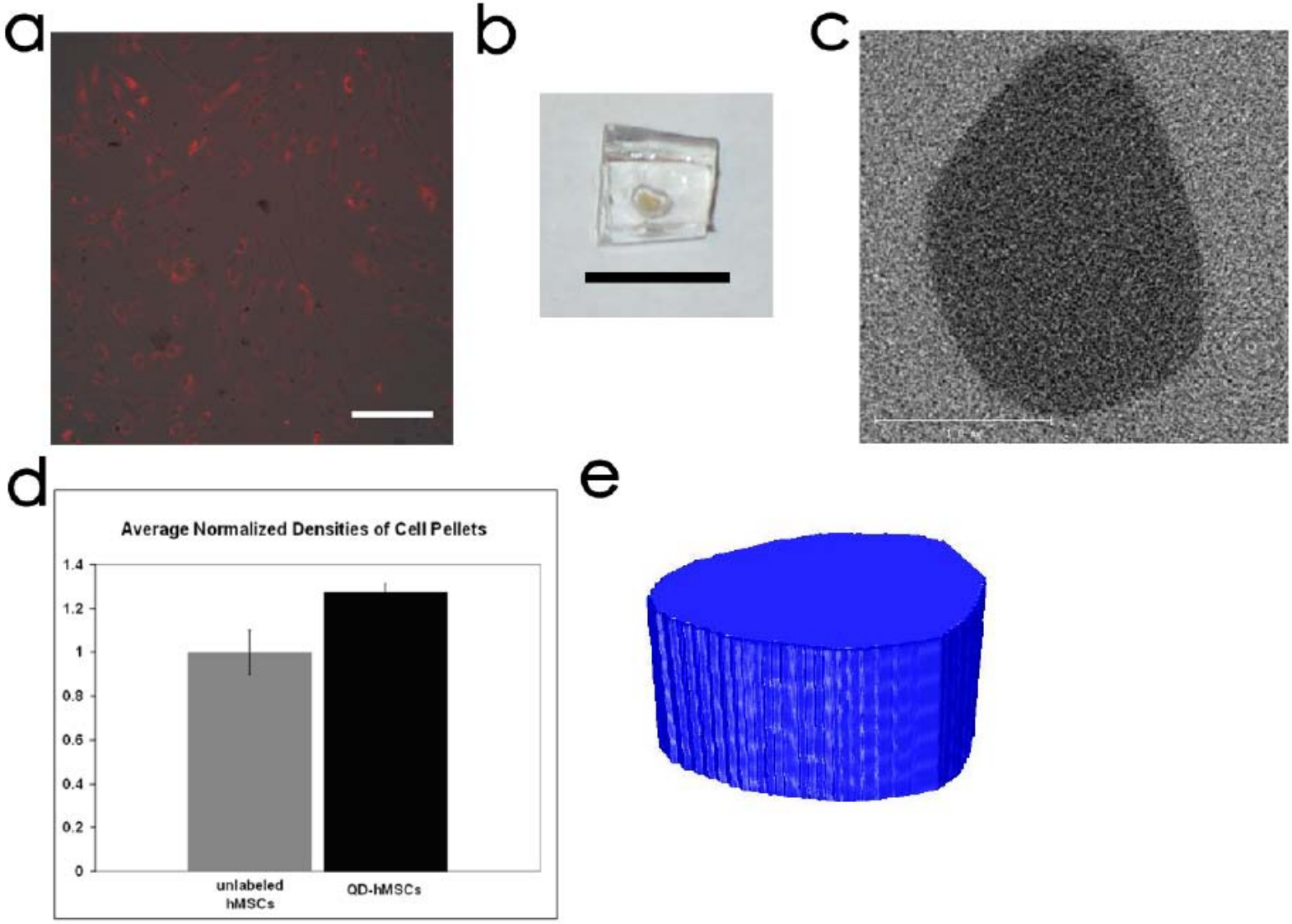
a
b
c
d
e
Average Normalized Densities of Cell Pellets
1.4
1.2
1
0.8
0.6
0.4
0.2
0
unlabeled hMSCs
QD-hMSCs

5 Conclusions and Future Directions

In this dissertation, we have identified a potential solution to the challenge of tracking exogenous stem cells in the heart. Quantum dots (QDs) are bright, photostable and have unique spectral features that mitigate the effects of autofluorescence when imaged in myocardium. We have developed a novel approach to stably label human mesenchymal stem cells (hMSCs) with QDs through an endocytotic-dependent passive loading process. The intracellular distribution of QDs remains cytoplasmically diffuse and fluorescence is sufficiently bright to permit imaging over at least 6 weeks (and at least 5 cell divisions) *in vitro*. Through a series of *in vitro* and *in vivo* experiments we have validated the use of QDs as a long-term vital stem cell labeling agent. Our data suggests that the QD label is retained only by the originally loaded cells and their progeny, and does not transfer to neighboring cells. Furthermore, the presence of QDs within cells does not affect their proliferative capacity. QD-hMSCs can be transfected with key pacemaker genes and express these genes similarly to unlabeled hMSCs. Finally, since the presence of QDs does not affect the differentiation capacity of hMSCs, the method is generalizable and can be used to study repair in other organ systems.

We injected QD-hMSCs into rat ventricles and generated complete 3-D reconstructions of the exogenous cellular distribution at 1-hour and 1-day after delivery. Analyses of these models suggest that individual stem cells do not wander significantly from the main cell cluster within the first 24-hours after injection. Interestingly, stem cell alignment does change over this time frame, with stem cell orientation mimicking that of the native tissue. Since gap junctions between hMSCs and myocytes can form within 24 hours, we suspect that the exogenous cells are forming a continuous syncytium with the endogenous myocytes.

In another set of *in vivo* experiments, we delivered QD-hMSCs to the canine heart via implantation on an extracellular scaffold. We were able to identify the delivered cells in histologic sections from tissue harvested 8 weeks after delivery. This suggests that QDs can be used for long term cell tracking *in vivo*. However, in order to locate our delivered cells, we sectioned several thousand microns worth of tissue and visually sampled slides at hundred-micron intervals. We identified the QD-positive regions several hundred-microns into the tissue, emphasizing the importance of careful sampling; many existing studies demonstrate findings from a single histologic section but in the absence of an unambiguous marker, it is very unlikely that a random section will contain any delivered cells. Had secondary staining been necessitated on all of these sections—as would have been the case for traditional cell tracking approaches—the process of identifying the delivered cells would have taken many months as opposed to several days. LeGrice, *et al*, have recently developed automated techniques for sectioning and subsequent confocal imaging of myocardial samples[69]. Such a system could be extended to image QD-hMSCs within a network of host tissue and even further streamline our approach.

Many investigators are interested in delivering stem cells for cardiac repair in the hopes that these cells will terminally differentiate into functional myocytes. In order to measure the efficacy of stem cell therapies for this purpose, it will therefore be necessary to locate the delivered cells several weeks to months after delivery and characterize their phenotype. Previous tools for tracking stem cells in vivo have failed because of high

levels of autofluorescence, inability to label nearly 100% of the delivered cells, or due to technical constraints (i.e., false positives, exhaustive secondary staining, cost). Now with QDs, not only can stem cells be identified in histologic sections with relative ease, but one can also stain for phenotypic markers of cardiac fate and probe for co-localization. Indeed, we have already found evidence of QD-hMSCs differentiating into endothelical cells and QD-cardiogenic cells differentiating into mature myocytes 8 weeks after delivery.

Our long-term goal is to develop cellular therapies for cardiovascular repair. QD tracking of cardiogenic cells *in vivo* over prolonged periods will allow us to identify the potential of these cells for cardiac regeneration. Although we have begun to identify some QD-cardiogenic cells that become myocytes *in vivo*, we must also consider their effects on the host tissue. If markers of cell proliferation are upregulated in native myocytes (ki67) and/or haematopoetic stem cells (c-kit^{+}) are recruited to the region of QD-cardiogenic cells, this would suggest that the delivered cells are altering the paracrine milieu of the tissue. Similarly, for cardiogenic cells to be effective as myocyte precursors they must develop terminal features that are appropriate to their physical location in the heart. We have already suggested that efforts should be made to determine whether therapeutic stem cells can respond to local cues and develop ventricular or atrial-specific fates after delivery to a given chamber[70]. Should a mismatch in the phenotype of differentiated exogenous cells and the chamber in which they reside be found, investigators must then consider the limitations of these therapies.

Although we demonstrated that QDs satisfy most of the requirements of an ideal tracking agent listed in Chapter 4.1, perhaps the most difficult goal to achieve is to extend this tool to permit non-invasive imaging. We have begun to explore several potential methods of live animal imaging, including our preliminary studies with μCT. Proof-of-concept experiments suggest that the net density increase afforded by the presence of QDs within the cytoplasm will allow QD-hMSCs to contrast sufficiently against host tissue in μCT scans. However, several experiments should be performed to validate that the method will work *in vivo* and (a more challenging obstacle) in a living, breathing animal. If this method does not succeed, we have envisoned other options for integrating QDs into a non-invasive imaging technique.

Several groups are currently using superparamagnetic iron oxide (SPIO) particles for non-invasive cell tracking *in vivo*[30, 34]. One group has even used fluorophore-conjugated SPIOs (what they termed iron fluorophore particles) as a labeling agent[63]. These approaches have certain limitations, including toxicity of magnetite to the cells, exocytosis of the label, potential for interference with differentiation, and difficulty in uniformly labeling a population of cells. Furthermore, although they permit non-invasive imaging, analysis of *ex vivo* samples is hindered by the need to perform secondary staining on histologic sections in order to identify the labeled cells (i.e. Prussian blue staining for iron).

Because we have already demonstrated that QDs are non-toxic, retained by loaded cells and can easily uniformly label millions of cells at a time, we have considered conjugating SPIOs to QDs as a unique dual-modality imaging approach. This approach relies on the binding of the molecules biotin and streptavidin, one of the strongest attractions in biology. Invitrogen manufactures QDs with the same size and charge compositions as those that we have used (655-nm, negatively-charged) with a

streptavidin moiety conjugated to the outer surface. We have successfully attempted passive loading of hMSCs with these dots and seen no qualitative differences between those cells and our standard QD-hMSCs (see Table 4.1.1). Biotin-coated magnetite nanoparticles are commercially available. By incubating biotin-SPIOs with streptavidin-QDs, it may be possible to create QD-SPIOs through biotin-streptavidin linkage. If these particles load into hMSCs similarly to plain QDs, then cells labeled with these dual-modal particles can be delivered to animals and their locations can be tracked over time non-invasively using magnetic resonance imaging (MRI). To validate the technique it would then be necessary to terminate the animals to confirm, by generating 3-D reconstructions of QDs in histologic sections, that the MR images appropriately describe the cellular distribution. In this way a non-invasive method of tracking the cells at low resolution (minimum of ~50,000 cells) could be developed and it would also be possible to understand behavior of single-cells using our existing custom algorithms. If deemed safe and effective in animals, it might also be more appropriate than traditional SPIOs as a tracking agent for use in Phase I clinical trials, as QD-SPIOs may be less toxic and less prone to leak out of cells.

Should QD-to-SPIO conjugation not be feasible, or should these hybrid particles preclude uptake by the stem cell (i.e. passive loading), it might also be sufficient to perform serial labeling of hMSCs with QDs and then with SPIOs. The later would have to be introduced into cells using a lipid vehicle, and would likely not label 100% of the cells. However, this method would permit non-invasive imaging (using MRI) and subsequent *ex vivo* analysis to validate the MRI results and perform follow-up histology.

There are additional agents that could be used to enable the non-invasive arm of imaging. One such approach involves loading cells with nanoparticles doped with ^{19}F[71]. Because of the unique relaxation properties of this fluoride isotope, it can be imaged quite sensitively using MRI. This agent would not be identifiable in histologic sections and therefore any studies using ^{19}F for non-invasive *in vivo* tracking should involve serial labeling of the cells with QDs.

Cell therapies are not limited to hMSCs. Many studies are underway investigating the use of embryonic stem cells[72], bone marrow progenitor cells[31], expanded side population cells[73], or skeletal myoblasts[31] to repair damaged heart tissue. In addition, many *in vitro* studies could benefit from more robust labeling and long term tracking of cells. Therefore, another extension of this work would be to test passive QD loading on other cell types and generalize the approach. We have already found that QDs are taken up by canine MSCs, fibroblasts and neonatal rat ventricular myocytes. Theoretically, any cell type capable of endocytosis should be loadable, although optimization of media constituents may be necessary.

What lies ahead for stem cell investigations is the potential to address a host of questions about normal physiology, disease mechanisms and therapeutics. Stem cells are likely to be involved in the future of cardiology and cardiovascular surgery, but to understand the safety and efficacy of any new therapeutics we must exhaustively account for the location and fate of all delivered cells in animal models. Although the community of researchers involved in using stem cells for cardiac repair agrees that traditional methods of cell tracking have failed, studies relying on these methods continue to advance toward clinical trials. So as to avoid tragic and unnecessary deaths (as was seen with gene therapy[74]), and to uphold the basic tenets of the scientific method, we must

be completely convinced of our results in animal studies before testing on human subjects. Although this may mean "finding needles in a haystack," QDs represent a promising solution illuminating the path toward achieving this goal.

6 References Cited

1. Thom, T., N. Haase, W. Rosamond, et al., *Heart disease and stroke statistics--2006 update: a report from the American Heart Association Statistics Committee and Stroke Statistics Subcommittee.* Circulation, 2006. **113**(6): p. e85-151.

2. Rosen, M.R., P.R. Brink, I.S. Cohen, et al., *Genes, stem cells and biological pacemakers.* Cardiovasc Res, 2004. **64**(1): p. 12-23.

3. Potapova, I., A. Plotnikov, Z. Lu, et al., *Human mesenchymal stem cells as a gene delivery system to create cardiac pacemakers.* Circ Res, 2004. **94**(7): p. 952-9.

4. von Harsdorf, R., P.A. Poole-Wilson, and R. Dietz, *Regenerative capacity of the myocardium: implications for treatment of heart failure.* Lancet, 2004. **363**(9417): p. 1306-13.

5. Orlic, D., J.M. Hill, and A.E. Arai, *Stem cells for myocardial regeneration.* Circ Res, 2002. **91**(12): p. 1092-102.

6. Potapova, I., Doronin, S., Kelly, D., Rosen, A., Schuldt, A., Lu, Zhongju., Guo, Yuanjian., Raptis, N., Towner, A., Robinson, R., Rosen, M., Brink, P., Gaudette, G., Cohen, I., *Functional Regeneration of the Canine Ventricle Using Adult Human Mesenchymal Stem Cells Committed In Vitro to a Cardiac Lineage.* Circulation, 2006. **99**(5): p. E19.

7. Frangioni, J.V. and R.J. Hajjar, *In vivo tracking of stem cells for clinical trials in cardiovascular disease.* Circulation, 2004. **110**(21): p. 3378-83.

8. Chang, G.Y., X. Xie, and J.C. Wu, *Overview of stem cells and imaging modalities for cardiovascular diseases.* J Nucl Cardiol, 2006. **13**(4): p. 554-69.

9. Chemaly, E.R., R. Yoneyama, J.V. Frangioni, et al., *Tracking stem cells in the cardiovascular system.* Trends Cardiovasc Med, 2005. **15**(8): p. 297-302.

10. Kehat, I., L. Khimovich, O. Caspi, et al., *Electromechanical integration of cardiomyocytes derived from human embryonic stem cells.* Nat Biotechnol, 2004. **22**(10): p. 1282-9.

11. Katritsis, D.G., P.A. Sotiropoulou, E. Karvouni, et al., *Transcoronary transplantation of autologous mesenchymal stem cells and endothelial progenitors into infarcted human myocardium.* Catheter Cardiovasc Interv, 2005. **65**(3): p. 321-9.

12. Yoon, Y.S., A. Wecker, L. Heyd, et al., *Clonally expanded novel multipotent stem cells from human bone marrow regenerate myocardium after myocardial infarction.* J Clin Invest, 2005. **115**(2): p. 326-38.

13. Maltsev, V.A., J. Rohwedel, J. Hescheler, et al., *Embryonic stem cells differentiate in vitro into cardiomyocytes representing sinusnodal, atrial and ventricular cell types.* Mech Dev, 1993. **44**(1): p. 41-50.

14. Shmelkov, S.V., S. Meeus, N. Moussazadeh, et al., *Cytokine preconditioning promotes codifferentiation of human fetal liver CD133+ stem cells into angiomyogenic tissue.* Circulation, 2005. **111**(9): p. 1175-83.

15. Jackson, K.A., S.M. Majka, G.G. Wulf, et al., *Stem cells: a minireview.* J Cell Biochem Suppl, 2002. **38**: p. 1-6.

16. Stocum, D.L., *Stem cells in regenerative biology and medicine.* Wound Repair Regen, 2001. **9**(6): p. 429-42.

17. Oh, H., S.B. Bradfute, T.D. Gallardo, et al., *Cardiac progenitor cells from adult myocardium: homing, differentiation, and fusion after infarction.* Proc Natl Acad Sci U S A, 2003. **100**(21): p. 12313-8.

18. Messina, E., L. De Angelis, G. Frati, et al., *Isolation and expansion of adult cardiac stem cells from human and murine heart.* Circ Res, 2004. **95**(9): p. 911-21.

19. Laugwitz, K.L., A. Moretti, J. Lam, et al., *Postnatal isl1+ cardioblasts enter fully differentiated cardiomyocyte lineages.* Nature, 2005. **433**(7026): p. 647-53.

20. Abeloff, M.D., *Clinical oncology*. 3rd ed. 2004, Philadelphia, Pa.: Elsevier/Churchill Livingstone. xxiv, 3205 p.

21. Pittenger, M.F. and B.J. Martin, *Mesenchymal stem cells and their potential as cardiac therapeutics.* Circ Res, 2004. **95**(1): p. 9-20.

22. Chen, S.L., W.W. Fang, J. Qian, et al., *Improvement of cardiac function after transplantation of autologous bone marrow mesenchymal stem cells in patients with acute myocardial infarction.* Chin Med J (Engl), 2004. **117**(10): p. 1443-8.

23. Meyer, G.P., K.C. Wollert, J. Lotz, et al., *Intracoronary bone marrow cell transfer after myocardial infarction: eighteen months' follow-up data from the randomized, controlled BOOST (BOne marrOw transfer to enhance ST-elevation infarct regeneration) trial.* Circulation, 2006. **113**(10): p. 1287-94.

24. Pittenger; Mark F., G.S.L., Mackay; Alastair Morgan, *Cardiac muscle regeneration using mesenchymal stem cells* in *http://patft.uspto.gov*, U.S. Patent, Editor. 2000, Osiris Therapeutics, Inc. : US.

25. Mazhari, R. and J.M. Hare, *Mechanisms of action of mesenchymal stem cells in cardiac repair: potential influences on the cardiac stem cell niche.* Nat Clin Pract Cardiovasc Med, 2007. **4 Suppl 1**: p. S21-6.

26. Billinton, N. and A.W. Knight, *Seeing the wood through the trees: a review of techniques for distinguishing green fluorescent protein from endogenous autofluorescence.* Anal Biochem, 2001. **291**(2): p. 175-97.

27. Laflamme, M.A. and C.E. Murry, *Regenerating the heart.* Nat Biotechnol, 2005. **23**(7): p. 845-56.

28. Jackson, K.A., S.M. Majka, H. Wang, et al., *Regeneration of ischemic cardiac muscle and vascular endothelium by adult stem cells.* J Clin Invest, 2001. **107**(11): p. 1395-402.

29. Kajstura, J., M. Rota, B. Whang, et al., *Bone marrow cells differentiate in cardiac cell lineages after infarction independently of cell fusion.* Circ Res, 2005. **96**(1): p. 127-37.

30. Kraitchman, D.L., A.W. Heldman, E. Atalar, et al., *In vivo magnetic resonance imaging of mesenchymal stem cells in myocardial infarction.* Circulation, 2003. **107**(18): p. 2290-3.

31. Thompson, R.B., S.M. Emani, B.H. Davis, et al., *Comparison of intracardiac cell transplantation: autologous skeletal myoblasts versus bone marrow cells.* Circulation, 2003. **108 Suppl 1**: p. II264-71.

32. Amado, L.C., A.P. Saliaris, K.H. Schuleri, et al., *Cardiac repair with intramyocardial injection of allogeneic mesenchymal stem cells after myocardial infarction.* Proc Natl Acad Sci U S A, 2005. **102**(32): p. 11474-9.

33. Dick, A.J., M.A. Guttman, V.K. Raman, et al., *Magnetic resonance fluoroscopy allows targeted delivery of mesenchymal stem cells to infarct borders in Swine.* Circulation, 2003. **108**(23): p. 2899-904.

34. Kraitchman, D.L., M. Tatsumi, W.D. Gilson, et al., *Dynamic imaging of allogeneic mesenchymal stem cells trafficking to myocardial infarction.* Circulation, 2005. **112**(10): p. 1451-61.

35. Barbash, I.M., P. Chouraqui, J. Baron, et al., *Systemic delivery of bone marrow-derived mesenchymal stem cells to the infarcted myocardium: feasibility, cell migration, and body distribution.* Circulation, 2003. **108**(7): p. 863-8.

36. Hofmann, M., K.C. Wollert, G.P. Meyer, et al., *Monitoring of bone marrow cell homing into the infarcted human myocardium.* Circulation, 2005. **111**(17): p. 2198-202.

37. Parish, C.R., *Fluorescent dyes for lymphocyte migration and proliferation studies.* Immunol Cell Biol, 1999. **77**(6): p. 499-508.

38. Bruchez, M., Jr., M. Moronne, P. Gin, et al., *Semiconductor nanocrystals as fluorescent biological labels.* Science, 1998. **281**(5385): p. 2013-6.

39. Chan, W.C. and S. Nie, *Quantum dot bioconjugates for ultrasensitive nonisotopic detection.* Science, 1998. **281**(5385): p. 2016-8.

40. Dubertret, B., P. Skourides, D.J. Norris, et al., *In vivo imaging of quantum dots encapsulated in phospholipid micelles.* Science, 2002. **298**(5599): p. 1759-62.

41. Rieger, S., R.P. Kulkarni, D. Darcy, et al., *Quantum dots are powerful multipurpose vital labeling agents in zebrafish embryos.* Dev Dyn, 2005. **234**(3): p. 670-81.

42. Jaiswal, J.K., H. Mattoussi, J.M. Mauro, et al., *Long-term multiple color imaging of live cells using quantum dot bioconjugates.* Nat Biotechnol, 2003. **21**(1): p. 47-51.

43. Wu, X., H. Liu, J. Liu, et al., *Immunofluorescent labeling of cancer marker Her2 and other cellular targets with semiconductor quantum dots.* Nat Biotechnol, 2003. **21**(1): p. 41-6.

44. Hanaki, K., A. Momo, T. Oku, et al., *Semiconductor quantum dot/albumin complex is a long-life and highly photostable endosome marker.* Biochem Biophys Res Commun, 2003. **302**(3): p. 496-501.

45. Silver, S.a.O., W., *Photoactivation of Quantum Dot Fluorescence Following Endocytosis.* Nano Letters, 2005. **5**(7): p. 1445-1449.

46. Zhang, Y.a.H., N., *Intracellular uptake of CdSe-ZnS/polystyrene nanobeads.* Journal of Biomedical Materials Research Part B: Applied Biomaterials, 2005. **76B**(1): p. 161-168.

47. Gao, X., Y. Cui, R.M. Levenson, et al., *In vivo cancer targeting and imaging with semiconductor quantum dots.* Nat Biotechnol, 2004. **22**(8): p. 969-76.

48. So, M.K., C. Xu, A.M. Loening, et al., *Self-illuminating quantum dot conjugates for in vivo imaging.* Nat Biotechnol, 2006. **24**(3): p. 339-43.

49. Derfus, A.M., W.C.W. Chan, and S.N. Bhatia, *Intracellular delivery of quantum dots for live cell labeling and organelle tracking.* Advanced Materials, 2004. **16**(12): p. 961-+.

50. Hoshino, A., K. Hanaki, K. Suzuki, et al., *Applications of T-lymphoma labeled with fluorescent quantum dots to cell tracing markers in mouse body.* Biochem Biophys Res Commun, 2004. **314**(1): p. 46-53.

51. Isenberg, G. and U. Klockner, *Calcium tolerant ventricular myocytes prepared by preincubation in a "KB medium".* Pflugers Arch, 1982. **395**(1): p. 6-18.

52. Cordeiro, J.M., L. Greene, C. Heilmann, et al., *Transmural heterogeneity of calcium activity and mechanical function in the canine left ventricle.* Am J Physiol Heart Circ Physiol, 2004. **286**(4): p. H1471-9.

53. Valiunas, V., S. Doronin, L. Valiuniene, et al., *Human mesenchymal stem cells make cardiac connexins and form functional gap junctions.* J Physiol, 2004. **555**(Pt 3): p. 617-26.

54. Derfus, A.M., Chan, W.C.W., and Bhatia, S.N., *Intracellular Delivery of Quantum Dots for Live Cell Labeling and Organelle Tracking.* Advanced Materials, 2004. **16**(12): p. 961-966.

55. Kuai, X.L., Bian, Y.H., Cong, X.Q., Li, X.L., Xiao, S.D, *Differentiation of mouse embryonic stem cells into hepatocytes in vitro and in vivo.* Chinese Journal of Digestive Diseases, 2003. **4**(2): p. 75-80.

56. Ballou, B., B.C. Lagerholm, L.A. Ernst, et al., *Noninvasive imaging of quantum dots in mice.* Bioconjug Chem, 2004. **15**(1): p. 79-86.

57. Abbas, A.K. and A.H. Lichtman, *Cellular and molecular immunology*. 5th ed. 2003, Philadelphia, PA: Saunders. 562 p.

58. Miyahara, Y., N. Nagaya, M. Kataoka, et al., *Monolayered mesenchymal stem cells repair scarred myocardium after myocardial infarction.* Nat Med, 2006. **12**(4): p. 459-65.

59. Kochupura, P.V., E.U. Azeloglu, D.J. Kelly, et al., *Tissue-engineered myocardial patch derived from extracellular matrix provides regional mechanical function.* Circulation, 2005. **112**(9 Suppl): p. I144-9.

60. Gaudette, G.R., J. Todaro, I.B. Krukenkamp, et al., *Computer aided speckle interferometry: a technique for measuring deformation of the surface of the heart.* Ann Biomed Eng, 2001. **29**(9): p. 775-80.

61. Cao, F., S. Lin, X. Xie, et al., *In vivo visualization of embryonic stem cell survival, proliferation, and migration after cardiac delivery.* Circulation, 2006. **113**(7): p. 1005-14.

62. MacLaren, D.C., T. Toyokuni, S.R. Cherry, et al., *PET imaging of transgene expression.* Biol Psychiatry, 2000. **48**(5): p. 337-48.

63. Hill, J.M., A.J. Dick, V.K. Raman, et al., *Serial cardiac magnetic resonance imaging of injected mesenchymal stem cells.* Circulation, 2003. **108**(8): p. 1009-14.

64. Aime, S., L. Calabi, C. Cavallotti, et al., *[Gd-AAZTA]-: a new structural entry for an improved generation of MRI contrast agents.* Inorg Chem, 2004. **43**(24): p. 7588-90.

65. Kostura, L., D.L. Kraitchman, A.M. Mackay, et al., *Feridex labeling of mesenchymal stem cells inhibits chondrogenesis but not adipogenesis or osteogenesis.* NMR Biomed, 2004. **17**(7): p. 513-7.

66. Arbab, A.S., G.T. Yocum, H. Kalish, et al., *Efficient magnetic cell labeling with protamine sulfate complexed to ferumoxides for cellular MRI.* Blood, 2004. **104**(4): p. 1217-23.

67. Bulte, J.W., D.L. Kraitchman, A.M. Mackay, et al., *Chondrogenic differentiation of mesenchymal stem cells is inhibited after magnetic labeling with ferumoxides.* Blood, 2004. **104**(10): p. 3410-2; author reply 3412-3.

68. Martin, E.T., J.A. Coman, F.G. Shellock, et al., *Magnetic resonance imaging and cardiac pacemaker safety at 1.5-Tesla.* J Am Coll Cardiol, 2004. **43**(7): p. 1315-24.

69. LeGrice, I., G. Sands, D. Hooks, et al., *Microscopic imaging of extended tissue volumes.* Clin Exp Pharmacol Physiol, 2004. **31**(12): p. 902-5.

70. Cohen, I.S., A.B. Rosen, and G.R. Gaudette, *A Caveat Emptor for myocardial regeneration: Mechanical without electrical recovery will not suffice.* J Mol Cell Cardiol, 2007. **42**(2): p. 285-8.

71. Ahrens, E.T., R. Flores, H. Xu, et al., *In vivo imaging platform for tracking immunotherapeutic cells.* Nat Biotechnol, 2005. **23**(8): p. 983-7.

72. Klug, M.G., M.H. Soonpaa, G.Y. Koh, et al., *Genetically selected cardiomyocytes from differentiating embronic stem cells form stable intracardiac grafts.* J Clin Invest, 1996. **98**(1): p. 216-24.

73. Beltrami, A.P., L. Barlucchi, D. Torella, et al., *Adult cardiac stem cells are multipotent and support myocardial regeneration.* Cell, 2003. **114**(6): p. 763-76.

74. Couzin, J. and J. Kaiser, *Gene therapy. As Gelsinger case ends, gene therapy suffers another blow.* Science, 2005. **307**(5712): p. 1028.

7 Appendix

```
% regQD.m
% This script takes as input a 2-D intensity image of QD+ cells (red fluorescence) in a
% section of tissue (phase).  Misregistration between successive images is assumed to be
% purely translation.  The user is prompted to select common points from
% image to image, which are collected in the matrix DispMat

numsect=154;
dnes=[];                    % include filename numbers for missing sections
%********************** FILE NAME INPUTS ************************
i=98;
j=1;
while i<=numsect
 if sum(i==dnes)==0
  else
  i=i+1
 end
 filename1=['3025_',num2str(i),'_(c2+c5).jpg'];
 I1=imread(filename1);
%********************** FIND NEW POINTS ************************
imshow(I1);
[x,y]=ginput(1);
DispMat(j,:)=[x y i];

j=j+1;
i=i+1;
 if sum(i==dnes)==0
  else
  i=i+1;
 end
end;

% moveims.m
% This script takes as input a 2-D intensity image of QD+ cells (red fluorescence) in a
% section of tissue (phase) and the DispMat output from the script regQD.m.
% Images are registered with respect to the first image index in the DispMat vector.

olddi=-142-268;
olddj=-62-228;
is=[801-olddj 1830-olddj];
js=[551-olddi 1850-olddi];
playmat=uint8(zeros(2630,2400,3));
%********************** FILE NAME INPUTS ********************
i=2;
while i<=length(DispMat(:,3))
```

```
 filename2=['3025_',num2str(DispMat(i,3)),'_(c2+c5).jpg'];
 im2=imread(filename2);
 regim=playmat;
 newpt=[DispMat(i,1,1) DispMat(i,2,1)];
 di=fix(newpt(1)-DispMat(1,1,1));
 dj=fix(newpt(2)-DispMat(1,2,1));
 if di>=is(1)
    di=is(1)-1;
 else
 end
 if dj>=js(1)
    dj=js(1)-1;
 else
 end
 regim(is(1)-dj:is(2)-dj, js(1)-di:js(2)-di,:)=im2;
 imwrite(regim, ['regim_',num2str(DispMat(i,3)),'.jpg']);
 clear im2, clear regim, clear newpt, clear trans*
 i=i+1;
end
```

```
% cropims.m
is=[400 2300];
js=[200 2400];
%******************** FILE NAME INPUTS **********************
i=1;
dnes=[];                    % include filename numbers for missing sections
while i<=154
 if sum(i==dnes)==0
  else
  i=i+1
 end
 filename=['regim_',num2str(i),'.jpg'];
 im=imread(filename);
 newim=im(is(1):is(2), js(1):js(2),:);
 imwrite(newim, ['regim_crop_',num2str(i),'.jpg']);
 clear im, clear newim
 i=i+1;
end
```

```
% QD3D_new.m
% This script takes as input a 2-D intensity image of QD+ cells (red fluorescence) in a
% section of tissue (phase).  The QD+ regions are identified and a new
% matrix is prepared, identifying these features.  The dot images are also
% translated to register with one another.  The input for this requires
% running regQD, moveims and cropims first.
```

```
DotMat=logical(zeros(380,440,154));
i=1;
numsect=126;
dnes=[];                                % include filename numbers for missing sections
while i<=numsect
   if sum(i==dnes)==0
   else
      i=i+1;
   end
 filename=['regim_crop_',num2str(i),'.jpg'];
 I1=imread(filename);                   % original image
%****************** FIND QD+ REGIONS ********************
 I1hsv=rgb2hsv(I1);                     % convert RGB to HSV
 sat=I1hsv(:,:,2); val=I1hsv(:,:,3);
 valxsat=immultiply(sat, val);          % binarize value matrix
 threshval=0.05;
dots=im2bw(valxsat, threshval);          % multiply binarized value x sat

%************* # PIXELS IN QD+ MATRIX ******************
QDsum(i)=sum(dots(:));
%************ ASSEMBLE 3D DOT MATRIX ****************

DotMat(:,:,i)=logical(imresize(dots,.2));
 clear I1*, clear dots, clear sat, clear val*
pack
i=i+1;
end
L=bwlabeln(DotMat);
figure, p=patch(isosurface(smooth3(L),.8));
set(p,'facecolor',[1,0,0],'edgecolor','none');
set(gca,'projection','perspective')
light('position',[1,1,1])
light('position',[-1,-1,-1])
light('position',[-1, 1,-1])
light('position',[ 1,-1,-1])
set(gca,'ZTickLabel',{'0.66';'';'1.06';'';'1.46';'';'1.86';''})
zlabel('mm','FontSize',24,'FontWeight','Bold')
set(gca,'XTick',[0 102.5010 205.0020 307.503 410.004])
set(gca,'XTickLabel',{'0';'0.5';'1.0';'1.5';'2.0'},'FontSize',24,'FontWeight','Bold')
set(gca,'YTick',[0 205.0020 410.004])
set(gca,'YTickLabel',{'0';'1.0';'2.0 '},'FontSize',24,'FontWeight','Bold')
xlabel('mm')
ylabel('mm')
```